



DEFORMATION MICROSTRUCTURES IN QUARTZO-FELDSPATHIC ROCKS

Jan Tullis

Brown University
jan_tullis@brown.edu

Holger Stunitz

Basel University
holger.stuenitz@unibas.ch

**Christian
Teyssier**

University of Minnesota
teyssier@tc.umn.edu

**Renee
Heilbronner**

Basel University
renee.heilbronner@unibas.ch

TABLE OF CONTENTS

[dedication](#)

[about the authors](#)

Tullis, J., Stunitz, H., Teyssier, C. and Heilbronner, R. 2000. Deformation Microstructures in Quartzo-feldspathic Rocks. In: Stress, Strain and Structure, A volume in honour of W D Means. Eds: M.W. Jessell and J.L.Urai. Volume 2, Journal of the Virtual Explorer. ISSN 1441-8126 (Print). ISSN 1441-8134 (CD-ROM). ISSN 1441-8126 (On-line at www.virtualexplorer.com.au/VEjournal/Volume2).

DEFORMATION MICROSTRUCTURES IN QUARTZO-FELDSPATHIC ROCKS

How to navigate

TABLE OF CONTENTS

Top page



From the title page you can reach the table of contents and the authors.

Table of contents



The table of contents page is the central page of the contribution. From there, all chapters can be reached.

Start of chapters



Each chapters starts with an introductory page. On it, you find:

- The title of the chapter.
- A light gray banner showing links to the top of the contribution and to the other chapters. This banner is the same on all introductory pages.
- A dark grey banner offering links to the sections of the chapter and back to the introductory page of the chapter (coloured field on the left of the banner). This banner is different for different chapters.
- An introductory text.
- Links to further readings and to the contributors of the thin sections.

Start of sections



Each section starts with a list of the microstructures described in the section. On that page, you find:

- The title of the chapter and the title of the section.
- A dark grey banner offering links to the other sections of the chapter and back to the introductory page of the chapter (same as on the introductory page). The current section is highlighted.
- Number of micrographs. Each number is also the name of the micrograph in the "Slides folder".
- Small icons showing the microstructures. The icons are linked to the corresponding images in the "Slides" folder.
- Titles (short captions) of the microstructures. The titles are linked to the corresponding descriptions (full captions) of the microstructures.

DEFORMATION MICROSTRUCTURES IN QUARTZO-FELDSPATHIC ROCKS

ACKNOWLEDGEMENTS

TABLE OF CONTENTS

We would also like to gratefully acknowledge our students, from whose theses many of the samples and photos were taken. These include

- Glen Shelton
- Andreas Kronenberg
- Lisa Dell'Angelo
- Greg Hirth
- Gayle Gleason
- Alice Post
- Jim Dunlap
- Michael Stipp
- Robert Kruse

We also wish to thank

- Jeanette Schaub

for undertaking the tedious job of scanning the slides and figuring out the scale bars...

TABLE OF CONTENTS

[TOP](#)

[PREFACE](#)

[authors](#)

[dedication](#)

- [i](#) [How to navigate](#)
- [ii](#) [... if you want to use this contribution as a book](#)
- [iii](#) [... if you want to use this contribution as a slide collection](#)

- [1](#) [Experimentally deformed quartz aggregates](#)
- [2](#) [Naturally deformed quartz-rich rocks](#)
- [3](#) [Experimentally deformed feldspar aggregates](#)
- [4](#) [Naturally deformed feldspar rocks](#)
- [5](#) [Experimentally deformed quartzo-feldspathic rocks](#)
- [6](#) [Naturally deformed quartzo-feldspathic rocks](#)
- [7](#) [Experimentally deformed pyroxenite and diabase](#)
- [8](#) [Deformation and metamorphic reactions in polyphase rocks](#)

- [iv](#) [Reference list](#)
- [v](#) [Acknowledgements](#)

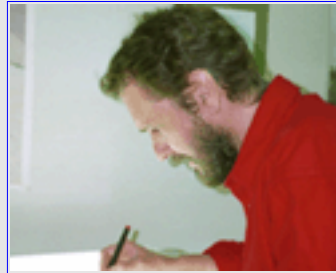
DEFORMATION MICROSTRUCTURES IN QUARTZO-FELDSPATHIC ROCKS

about the authors

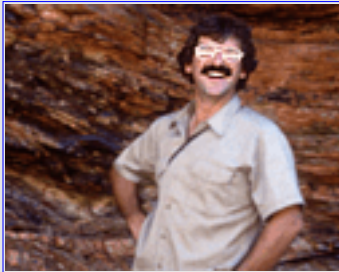
TABLE OF CONTENTS



Jan Tullis



Holger Stünitz



**Christian
Teyssier**



**Renée
Heilbronner**

[Acknowledgements](#)

DEFORMATION MICROSTRUCTURES IN QUARTZO-FELDSPATHIC ROCKS

... if you want to use this contribution as a book

TABLE OF CONTENTS

The contribution has been designed for **Netscape 4.7**, and comes out best if **standard settings** are used.

If you want to print a hardcopy version of this contribution you need to print

- **all HTML files** in the "**SlideSet**" folder and
- **all JPEG files** in the "**Slides**" folder.



"SlideSet": folder containing the description of the microstructures.

The descriptions of the thin sections (extended figure captions) have been grouped into eight chapters, each being saved in its own folder.

1. Experimentally deformed quartz aggregates
2. Naturally deformed quartz-rich rocks
3. Experimentally deformed feldspar aggregates
4. Naturally deformed feldspar rocks
5. Experimentally deformed quartzo-feldspathic rocks
6. Naturally deformed quartzo-feldspathic rocks
7. Experimentally deformed pyroxenite and diabase
8. Deformation and metamorphic reactions in polyphase rocks

Each chapter begins with an introductory page and consists of a number of sections. Each section corresponds to a deformation regime (sometimes two regimes are combined into one).

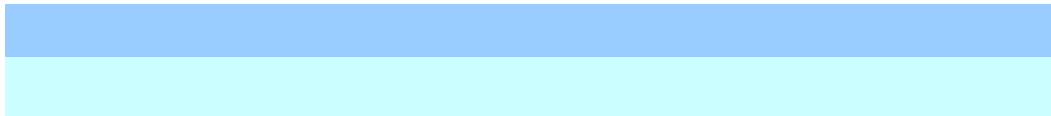
Each section begins with the list of microstructures, followed by the full description of each of the microstructures.



"Slides": folder containing 97 photomicrographs of microstructures.

Most of these images have been taken from a collection of thin sections which were used in a GSA short course ("Deformation Mechanisms and Microstructures", October 1998).

The micrographs have been scanned and saved as 1800x1200 JPEG colour images. Some processing has been applied to them and all images have a scale bar, indicating the true size.



DEFORMATION MICROSTRUCTURES IN QUARTZO-FELDSPATHIC ROCKS

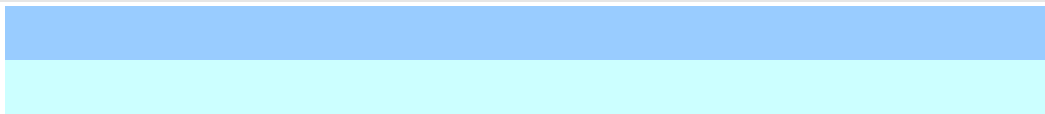
DEDICATION

TABLE OF CONTENTS

All four of us are very pleased to dedicate this contribution to our dear friend and respected colleague Win Means. Win has been an inspiration to us in so many ways. His innovative and provocative 'see-through' experiments on analog materials have had an enormous impact on how we think about the evolution and significance of microstructures in experimentally and naturally deformed 'real rocks', where all we can observe is the final snapshot. In this contribution, however, we do not compete with him and his closest disciples in the field of see-through experiments. All we offer are pictures of naturally and experimentally produced deformation microstructures. Maybe experimental deformation performed on real rocks is closer to nature than analogue modelling applied to synthetic materials - maybe it only confuses us more by its many complexities. Be that how it may, by placing this collection of real rock microstructures on this CD we hope that readers (or should we say viewers...?) are both reminded of the "real world" and also encouraged to apply a "Meansian" clear-sightedness to it. Because of this we are sure: that the way of looking at things, the ways of seeing and understanding must always be the same in all cases. And the way of seeing the real world - of seeing it through analogues - that Win has taught us will further our understanding of microstructure for some time to come.

Wins textbooks and short course notes and tapes and CDs have allowed a huge improvement in the teaching of stress and strain and other aspects of structural geology. His thoughtful questions and insightful comments have helped so many of us to improve our manuscripts and to clarify our thinking about the problems we are working on. His talks are models of effective communication: at first they may appear deceptively simple, but Win actively engages and gently challenges his listeners, so that they really learn, and remember, something new. Win is the most generous person we know with his time, as a teacher, mentor, reviewer, and friend, and

he is unfailingly positive and constructive in his suggestions. It is good to know that it is possible to be a first rate scientist as well as a wonderful person. Thank you, Win, for the difference you have made - and still make - in our science and in our lives!



DEFORMATION MICROSTRUCTURES IN QUARTZO-FELDSPATHIC ROCKS

PREFACE

TABLE OF CONTENTS

In the past decade there has been enormous progress in our understanding of the deformation mechanisms and rheology of Earth materials, due to progress in experimental rock deformation studies as well as detailed studies of naturally deformed rocks from well-characterized settings. Microstructures form the link between experimentalists and field geologists, and similarities of microstructures provide the principal criterion for inferring operation of the same process, although at quite different conditions. We now can have reasonable confidence in using the microstructures in naturally deformed rocks to extract useful information about the deformation conditions. Thus it seemed a good time to compile some examples of deformation microstructures from experimentally and naturally deformed samples, as well as our interpretations of them, to illustrate some important processes of rock deformation. These may serve as a reference and teaching tool for Earth scientists interested in rock deformation as well as providing a starting point for further discussion among researchers in this field (who may or may not agree with our interpretations). Naturally, such a small collection of only 100 photos can only present a few examples, and is biased by the preferences and perspectives of the authors.

These images illustrate optical microstructures resulting from a variety of deformation processes that are operative in the crust, ranging from localized faulting to distributed microcracking to pressure solution to dislocation creep to grain boundary sliding and diffusion creep, with and without accompanying phase changes. However most of the images illustrate microstructures produced by dislocation creep, because this is perhaps the dominant deformation mechanism in the mid to lower crust, and also has been well studied experimentally.

We have included a very selective reference list for further reading which is referred to at the end of the introductions to the chapters. This list is by no means complete or in any way representative. It

reflects the research interests of the contributors.

Experimental studies on quartz aggregates have identified three distinct regimes of dislocation creep, defined by different mechanisms of dynamic recrystallization. These regimes are operative at different temperature-strain rate conditions, and produce different mechanical behavior, and they result in distinctively different microstructures. These same distinct microstructures have been recognized in naturally deformed quartzites, although at much lower temperatures at the slower natural strain rates. The lowest temperature dislocation creep regime has also been identified in experimentally deformed feldspars, and the higher temperature regimes have been inferred from the microstructures of high grade naturally deformed anorthosites. Thus it may be possible to infer the temperature or strain rate of the natural deformation from analysis of the dislocation creep microstructures in quartzo-feldspathic rocks and comparison with experimentally deformed samples. We hope that the images we have collected here of experimentally and naturally deformed quartzo-feldspathic aggregates will help people to recognize and distinguish the microstructures produced by the three different mechanisms of recrystallization in these two minerals.

Another very important microstructural parameter is the size of dynamically recrystallized grains, which is largely dependent on the flow stress in single phase aggregates. Thus the recrystallized grain size may provide a paleopiezometer by which the flow stress can be inferred. If such flow stress estimates are combined with information about the temperature or strain rate inferred from the dislocation creep regime microstructures, plus experimental flow laws, we can begin to put good constraints on the deformation conditions. Obviously great caution is necessary in making such inferences; however, we believe the prospects are promising, and can only improve as field geologists provide feedback to experimentalists as to how good or bad the match appears to be!

This collection of images concentrates on the deformation microstructures of quartzo-feldspathic rocks. The examples start with experimentally deformed samples, because in experiments the deformation conditions of pressure, temperature and strain rate (as well as chemical environment) can be controlled, and therefore the dependence of microstructures on ambient deformation conditions can be well demonstrated. The images of naturally deformed aggregates which follow each set of images of experimentally deformed samples have been chosen to illustrate a wide range of similar features that have been found in many rocks. The collection starts with microstructures developed in single phase aggregates of quartz, and then of feldspar, and then progresses to include polyphase quartzo-feldspathic aggregates. The natural deformation of polyphase aggregates often includes the additional complication

of chemical disequilibrium and metamorphic phase changes, which may in turn have significant effects on the deformation by allowing a switch in the dominant deformation mechanism to grain boundary sliding and diffusion creep. A few examples of this situation have been included.

Apart from the wealth of information that can be derived from a microstructural analysis of rocks, the microstructures themselves are often very beautiful. Thus we hope that this collection serves not only as a useful teaching tool but that it is also pleasant to look at, and in this way we can contribute to what (Earth) science should be: fun!

[further reading](#)

DEFORMATION MICROSTRUCTURES IN QUARTZO-FELDSPATHIC ROCKS

Reference list

TABLE OF CONTENTS

Preface

Dunlap, W.J., Hirth, G. and Teyssier, C., 1997, Thermomechanical evolution of a ductile duplex. *Tectonics*, 16, 983-1000.

Hirth, G., and Tullis, J., 1992, Dislocation creep regimes in quartz aggregates: *Jour. Struc. Geol.*, 14, 145-160.

Snoke, A.W. and Tullis, J., 1998, An overview of fault rocks. in *Fault-Related Rocks: A Photographic Atlas*, A. Snoke, J. Tullis & V. Todd, eds., Princeton Univ. Press, 3-18.

Experimentally deformed quartz aggregates

Dell'Angelo, L.N. and Tullis, J., 1989, Fabric development in experimentally sheared quartzites. *Tectonophys.*, 169, 1-21.

Gleason, G.C., Tullis, J. and Heidelbach, F.M., 1993, The role of dynamic recrystallization in the development of lattice preferred orientations in experimentally deformed quartz aggregates. *Jour. Struc. Geol.*, 15, 1145-1168.

Hirth, G. and Tullis, J., 1994, The nature of the brittle to plastic transition in quartz aggregates. *Jour. Geophys. Res.*, 99, 11731-11748.

Hirth, G., and Tullis, J., 1992, Dislocation creep regimes in quartz aggregates: *Jour. Struc. Geol.*, 14, 145-160.

Tullis, J. and Gleason, G., 1998, Effects of static annealing on experimentally deformed quartzite and aplite, in *Fault-Related Rocks: A Photographic Atlas*. A. Snoke, J. Tullis & V. Todd, eds., Princeton Univ. Press, 462-463.

Naturally deformed quartz-rich rocks

Dunlap, W.J., Hirth, G. and Teyssier, C., 1997, Thermomechanical evolution of a ductile duplex. *Tectonics*, 16, 983-1000.

Hirth, G., Teyssier, C. and Dunlap, W.J., An evaluation of quartzite flow laws based on comparisons between experimentally and naturally deformed rocks, In press, *Geol. Rundsch.*

van Daalen, M., Heilbronner, R. & Kunze, K. 1999. Orientation analysis of localized shear deformation in quartz fibres at the brittle-ductile transition. *Tectonophysics* 303, 83-108.

Pauli, C., Schmid, S. M. & Panozzo Heilbronner, R. 1996. Fabric domains in quartz mylonites: localized three dimensional analysis of microstructure and texture. *J. Structural Geology* 18, 1183-1203.

Experimentally deformed feldspar aggregates

Post, A.D. and Tullis, J., 1999, A recrystallized grain size piezometer for experimentally deformed feldspar aggregates. *Tectonophys.*, 303, 159-173.

Tullis, J. and Yund, R.A., 1987, Transition from cataclastic flow to dislocation creep of feldspar: mechanisms and microstructures: *Geology*, 15, 606-609.

Tullis, J., and Yund, R.A., 1992, The brittle-ductile transition in feldspar aggregates: an experimental study: in, *Fault Mechanics and Transport Properties of Rocks*, B. Evans & T.-f. Wong, eds., Academic Press, NY, 89-118.

Tullis, J. and Yund, R.A., 1985, Dynamic recrystallization of feldspar: a mechanism for ductile shear zone formation: *Geology*, 13, 238-241.

Tullis, J., Dell'Angelo, L.N., and Yund, R.A., 1990, Ductile shear zones from brittle precursors in feldspathic rocks; the possible role of dynamic recrystallization: in *The Brittle-Ductile Transition: The Heard Volume*, A. Duba, W. Durham, J. Handin, and H. Wang, eds., , Amer. Geophys. Union Monograph 56, 67-82.

Yund, R.A., and Tullis, J., 1991, Compositional changes of minerals associated with dynamic recrystallization. *Contrib. Mineral. Petrol.*, 108, 346-355.

Naturally deformed feldspar rocks

Kruse, R., and Stunitz, H., 1999, Deformation mechanisms and phase distribution in mafic high-temperature mylonites from the

Jotun Nappe, southern Norway. *Tectonophys.*, 303, 223-249.

Stunitz, H., 1998, Syn-deformational recrystallization - dynamic or compositionally induced? *Contrib. Mineral. Petrol.*, 131, 219-236.

Experimentally deformed quartzo-feldspathic rocks

Dell'Angelo, L.N. and Tullis, J., 1996, Textural and mechanical evolution with progressive strain in experimentally deformed aplite. *Tectonophysics*, 256, 57-82.

Tullis, J., Dell'Angelo, L.N., and Yund, R.A., 1990, Ductile shear zones from brittle precursors in feldspathic rocks; the possible role of dynamic recrystallization: in *The Brittle-Ductile Transition: The Heard Volume*, A. Duba, W. Durham, J. Handin, and H. Wang, eds., Amer. Geophys. Union Monograph 56, 67-82.

Tullis, J. and Gleason, G., 1998, Effects of static annealing on experimentally deformed quartzite and aplite, in *Fault-Related Rocks: A Photographic Atlas*. A. Snoke, J. Tullis & V. Todd, eds., Princeton Univ. Press, 462-463.

Dell'Angelo, L.N. and Tullis, J., 1988, An experimental study of the effect of partial melt on granitic aggregates deformed at high pressures and temperatures: *Jour. Met. Geol.*, 6, 495-516.

Experimentally deformed pyroxenite and diabase

Tullis, T.E., Horowitz, F.E. and Tullis, J., 1991, Flow laws of polyphase aggregates from end member flow laws. *Jour. Geophys. Res.*, 96, 8081-8096.

Kronenberg, A.K. and Shelton, G.S., 1980, Deformation microstructures in experimentally deformed Maryland diabase. *Jour. Struc. Geol.*, 2, 341-353.

Deformation and metamorphic reactions in polyphase rocks

Fitz Gerald, J.D. and Stunitz, H., 1993, Deformation of granitoids at low metamorphic grade. I. Reactions and grain size reduction. *Tectonophys.*, 221, 269-297.

Kruse, R., and Stunitz, H., 1999, Deformation mechanisms and phase distribution in mafic high-temperature mylonites from the Jotun Nappe, southern Norway. *Tectonophys.*, 303, 223-249.

Stunitz, H. and Tullis, J., Weakening and strain localization produced by syndeformational reaction of plagioclase. In press, Geol. Rundsch.

Stunitz, H., 1993, Transition from fracturing to viscous flow in a naturally deformed metagabbro. in Defects and Processes in the Solid State: Geoscience Applications, J.N. Boland and J.D. Fitz Gerald, eds., Elsevier, Amsterdam, 121-150.

Stunitz, H. and Fitz Gerald, J.D., 1993, Deformation of granitoids at low metamorphic grades. II. Granular flow in albite-rich mylonites. Tectonophys., 221, 299-324.

Stunitz, H., 1998, Syn-deformational recrystallization - dynamic or compositionally induced? Contrib. Mineral. Petrol., 131, 219-236.

DEFORMATION MICROSTRUCTURES IN QUARTZO-FELDSPATHIC ROCKS

.. if you want to use this contribution as a
slide collection

TABLE OF CONTENTS

Complete list of microstructures

To obtain a hardcopy of the complete list of microstructures the following files should be printed (they can be found in the eight folders (chapters) in the "**SlideSet**" folder):

1. exdqa_start.html
2. exdqa_semi.html
3. exdqa_reg2.html
4. exdqa_reg3.html
5. exdqa_anneal.html
1. natdqrr_undef.html
2. natdqrr_semi_blg.html
3. natdqrr_sgr.html
4. natdqrr_gbm.html
1. exdfa_start.html
2. exdfa_cata.html
3. exdfa_reg1.html
1. natdfr_reg1.html
2. natdfr_low_reg2.html
3. natdfr_high_reg2.html
1. exdfgg_start_reg1.html
2. exdfgg_reg2.html
3. exdfgg_ann_melt.html
1. natdqr_low_MF.html
2. natdqr_high_MF.html
3. natdqr_mylo_RB.html
4. natdqr_ultra_RB.html
1. exdp_exdd_.html

1. Dmrpr_grano.html
2. Dmrpr_anortho_.html

The full-size images of the thin sections are stored in the "**Slides**" folder. Dragging the folder "**DeformationMicrostructure**" into the open window of Netscape will display this file structure. Opening "**Slides**" from here will allow you to page through the collection.



1

Experimentally deformed quartz aggregates

TOP

- | | |
|---|--|
| <u>1-</u> Experimentally deformed quartz aggregates | <u>2-</u> Naturally deformed quartz-rich rocks |
| <u>3-</u> Experimentally deformed feldspar aggregates | <u>4-</u> Naturally deformed feldspar rocks |
| <u>5-</u> Experimentally deformed quartzo-feldspathic rocks | <u>6-</u> Naturally deformed quartzo-feldspathic rocks |
| <u>7-</u> Experimentally deformed pyroxenite and diabase | <u>8-</u> Deformation and metamorphic reactions in polyphase rocks |

Experimentally deformed quartz aggregates

starting materials / semi-brittle & regime 1 / regime 2 / regime 2 & 3 / annealing

Introduction

The goal of experimental deformation studies is to activate the same processes that occur in nature, but under known and controlled conditions. In order to activate crystal plastic deformation processes at relatively fast laboratory strain rates ($10^{-4}/\text{sec}$ to $10^{-7}/\text{sec}$), experiments are done at higher temperatures and confining pressures (and thus water fugacities) than those in nature. Most experiments on quartz aggregates have been done 'as-is', with the naturally occurring water content of $\sim 0.1\text{-}0.2$ wt%, but for some a small amount ($\sim 0.1\text{-}0.2$ wt%) of water was added, to investigate the effect of this important variable. Over the range of experimental strain rates, addition of ~ 0.15 wt% water has approximately the same effect on dislocation creep strengths as increasing the temperature by 100°C .

Most of the experimentally deformed samples illustrated in this chapter have been subjected to axial compression at a constant strain rate, and the compression direction in the photos is vertical. The samples start out as cylinders 6.3mm (0.25") in diameter and $\sim 15\text{mm}$ (0.6") long; they are shortened by up to 65%. The photos have been taken from the center portions of the samples. One sample was subjected to a combination of compression and shear, using pistons cut at 45° to the apparatus compression direction. At the end of most deformation experiments, the temperature is rapidly quenched (down to 300°C in < 2 minutes) while the sample remains under differential stress, in order to preserve the deformation microstructures. However at the end of a few experiments, the differential stress was removed and the sample was allowed to remain at P and T, to study the effects of static annealing.

Many photos of experimentally deformed samples show horizontal

extension cracks; these result from decompression at the end of the experiments, after deformation and quenching. The thin sections are extra thin and doubly polished, in order to more clearly show details of small recrystallized grains.

The photos in this chapter illustrate the transition from semi-brittle flow (distributed microcracks and dislocations) to crack-free dislocation creep, which occurs with increasing temperature or decreasing strain rate (and thus with decreasing flow stress). As explained briefly in the Preface to this contribution, three microstructurally distinct regimes of dislocation creep, associated with distinct processes of dynamic recrystallization, have been identified in experimentally quartz aggregates, and these same regimes have been recognized in quartz aggregates naturally deformed at lower temperatures and slower strain rates. The distinctions between these regimes are explained more fully in the individual photo captions. One image illustrates the asymmetry in microstructures that results from a component of simple shear, and another pair of images illustrates the effect of static annealing after deformation.

[further reading](#)

Experimentally deformed quartz aggregates

Further reading

Experimentally deformed quartz aggregates

starting materials / semi-brittle & regime 1 / regime 2 / regime 2 & 3 / annealing

Dell'Angelo, L.N. and Tullis, J., 1989, Fabric development in experimentally sheared quartzites. *Tectonophys.*, 169, 1-21.

Gleason, G.C., Tullis, J. and Heidelbach, F.M., 1993, The role of dynamic recrystallization in the development of lattice preferred orientations in experimentally deformed quartz aggregates. *Jour. Struc. Geol.*, 15, 1145-1168.

Hirth, G. and Tullis, J., 1994, The nature of the brittle to plastic transition in quartz aggregates. *Jour. Geophys. Res.*, 99, 11731-11748.

Hirth, G., and Tullis, J., 1992, Dislocation creep regimes in quartz aggregates: *Jour. Struc. Geol.*, 14, 145-160.

Tullis, J. and Gleason, G., 1998, Effects of static annealing on experimentally deformed quartzite and aplite, in *Fault-Related Rocks: A Photographic Atlas*. A. Snoke, J. Tullis & V. Todd, eds., Princeton Univ. Press, 462-463.

Experimentally deformed quartz aggregates

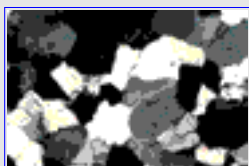
Starting materials

Experimentally deformed quartz aggregates

[starting materials](#) / [semi-brittle & regime 1](#) / [regime 2](#) / [regime 2 & 3](#) / [annealing](#)

List of microstructures

1



[Heavitree quartzite \(HQ\) starting material.](#)

5



[Black Hills quartzite \(BHQ\) starting material.](#)

Experimentally deformed quartz aggregates

Regime 2

Experimentally deformed quartz aggregates

[starting materials](#) / [semi-brittle & regime 1](#) / [regime 2](#) / [regime 2 & 3](#) / [annealing](#)

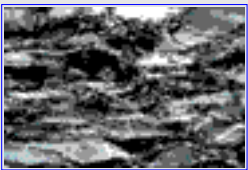
List of microstructures

3



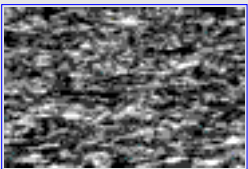
[HQ shortened 42% at 800°C, 10-6/sec and 1200 MPa; regime 2 dislocation creep.](#)

4



[HQ shortened 64% at 800°C, 10-6/sec and 1200 MPa; regime 2 dislocation creep.](#)

6



[BHQ shortened 50% at 800°C, 10-6/sec and 1200 MPa \('wet'\); regime 2 dislocation creep.](#)

7



[BHQ deformed by a combination of sinistral simple shear \(\$\gamma = 2.1\$ \) and shortening \(~50%\) at 800°C, 10-5/sec and 1200 MPa; regime 2 dislocation creep.](#)

Experimentally deformed quartz aggregates

Transition regime 2/3, regime 3

Experimentally deformed quartz aggregates

[starting materials](#) / [semi-brittle & regime 1](#) / [regime 2](#) / [regime 2 & 3](#) / [annealing](#)

List of microstructures

8



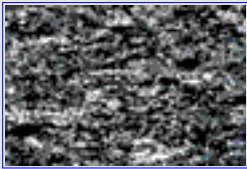
[BHQ shortened 30% at 900°C, 10-6/sec and 1200 MPa \('wet'\); transition between regime 2-3 dislocation creep.](#)

9



[BHQ shortened 37% at 900°C, 10-6/sec and 1200 MPa \('wet'\); transition between regime 2 - 3 dislocation creep.](#)

10



[BHQ shortened 57% at 900°C, 10-6/sec and 1200 MPa \('wet'\); transition between regime 2 - 3 dislocation creep.](#)

11



[Arkansas novaculite \(original d = 5 μm\) shortened 54% at 900°C, 10-6/sec and 1200 MPa \('wet'\); transition between regime 2 - 3 dislocation creep.](#)

12



[BHQ shortened 50% at 1200°C, 10-6/sec and 1200 MPa; regime 3 dislocation creep.](#)

Experimentally deformed quartz aggregates

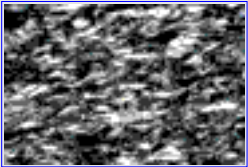
Effect of annealing

Experimentally deformed quartz aggregates

starting materials / semi-brittle & regime 1 / regime 2 / regime 2 & 3 / annealing

List of microstructures

13



BHQ shortened 60% at 800°C, 10⁻⁶/sec and 1200 MPa; regime 2 dislocation creep.

14



BHQ shortened 60% at 800°C, 10⁻⁶/sec and 1200 MPa (regime 2 dislocation creep); then annealed at 900°C for 120 hrs.

Experimentally deformed quartz aggregates

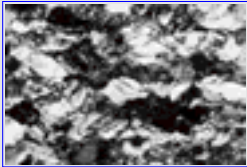
semi-brittle behaviour & regime 1

Experimentally deformed quartz aggregates

starting materials / semi-brittle & regime 1 / regime 2 / regime 2 & 3 / annealing

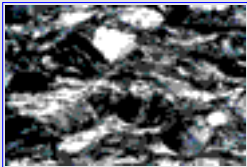
List of microstructures

21



HQ, shortened 50% at 700°C, 10⁻⁵/sec and 1200 MPa, in the semi-brittle flow regime.

2



HQ shortened 65% at 850°C, 10⁻⁵/sec and 1200 MPa; regime 1 dislocation creep.

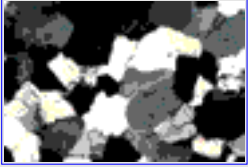
Experimentally deformed quartz aggregates

Figure caption

[Experimentally deformed quartz aggregates](#)

[starting materials](#) / [semi-brittle & regime 1](#) / [regime 2](#) / [regime 2 & 3](#) / [annealing](#)

1



Heavitree quartzite (HQ) starting material.

Heavitree quartzite (HQ) starting material from Australia. Non-porous quartzite, with ~1% impurities (muscovite, feldspar and iron oxides), and equant grains with average diameter ~200 μm . Intragranular water ~0.2 wt%, mostly in the form of fluid inclusions. Diagenetic overgrowths visible.

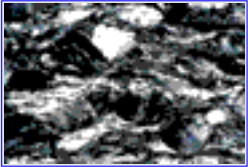
Experimentally deformed quartz aggregates

Figure caption

Experimentally deformed quartz aggregates

starting materials / semi-brittle & regime 1 / regime 2 / regime 2 & 3 / annealing

2



HQ shortened 65% at 850°C, 10⁻⁵/sec and 1200 MPa; regime 1 dislocation creep.

HQ shortened 65% at 850°C, 10⁻⁵/sec and 1200 MPa, in the lowest temperature dislocation creep regime (regime 1 of Hirth & Tullis, 1992). Temperature is too low for dislocation climb to operate as a recovery process. Strain is very inhomogeneous on the grain scale; parts of original grains remain as augen, whereas other parts appear as thin irregular ribbons. The undulatory extinction is strong and patchy. Dynamically recrystallized grains form by grain boundary migration but are extremely small ($d \sim 1 \mu\text{m}$) and thus are not resolvable optically. (W374)

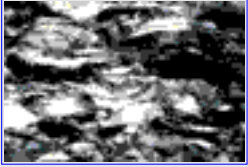
Experimentally deformed quartz aggregates

Figure caption

Experimentally deformed quartz aggregates

starting materials / semi-brittle & regime 1 / regime 2 / regime 2 & 3 / annealing

3



HQ shortened 42% at 800°C, 10⁻⁶/sec and 1200 MPa; regime 2 dislocation creep.

HQ shortened 42% at 800°C, 10⁻⁶/sec and 1200 MPa, in the intermediate temperature dislocation creep regime (regime 2 of H & T). Temperature is high enough for dislocation climb to serve as the recovery process. Original grains have been fairly homogeneously flattened, and exhibit smooth and continuous undulatory extinction; sub-basal deformation lamellae are quite common (e.g. faint sub-parallel traces in white grain just NE of scale bar). Recrystallized grains form at original grain boundaries as a result of progressive subgrain misorientation. In this regime the subgrains and the recrystallized grains have about the same size, but both are too fine (~3-5 μm) to resolve optically in this photo. (W339)

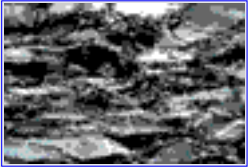
Experimentally deformed quartz aggregates

Figure caption

Experimentally deformed quartz aggregates

starting materials / semi-brittle & regime 1 / regime 2 / regime 2 & 3 / annealing

4



HQ shortened 64% at 800°C, 10⁻⁶/sec and 1200 MPa; regime 2 dislocation creep.

HQ shortened 64% at 800°C, 10⁻⁶/sec and 1200 MPa (regime 2 dislocation creep). This higher strain sample also shows moderately homogeneous flattening of original grains. There is a greater volume % of recrystallized grains, again mostly located on original grain boundaries. The 'puckered' appearance within many original grains is due to subgrains.

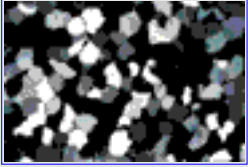
Experimentally deformed quartz aggregates

Figure caption

[Experimentally deformed quartz aggregates](#)

[starting materials](#) / [semi-brittle & regime 1](#) / [regime 2](#) / [regime 2 & 3](#) / [annealing](#)

5



Black Hills quartzite (BHQ) starting material.

Black Hills quartzite (BHQ) starting material, from South Dakota. Quartzite with up to 1% porosity and <1% iron oxides. Equant grains have an average diameter of ~100 μm .

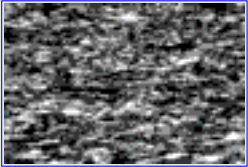
Experimentally deformed quartz aggregates

Figure caption

[Experimentally deformed quartz aggregates](#)

[starting materials](#) / [semi-brittle & regime 1](#) / [regime 2](#) / [regime 2 & 3](#) / [annealing](#)

6



BHQ shortened 50% at 800°C, 10⁻⁶/sec and 1200 MPa ('wet'); regime 2 dislocation creep.

BHQ shortened 50% at 800°C, 10⁻⁶/sec and 1200 MPa, with ~0.2 wt % water added. (The added water has the same effect as increasing the deformation temperature by ~100°C.) Deformation occurred by regime 2 dislocation creep; note the homogeneously flattened original grains. The recrystallized grains are larger and more abundant than those in photo #4 because of the added water. (BA20)

Experimentally deformed quartz aggregates

Figure caption

Experimentally deformed quartz aggregates

starting materials / semi-brittle & regime 1 / regime 2 / regime 2 & 3 / annealing

7



BHQ deformed by a combination of sinistral simple shear ($\gamma = 2.1$) and shortening (~50%) at 800°C, 10⁻⁵/sec and 1200 MPa; regime 2 dislocation creep.

BHQ deformed by a combination of simple shear ($\gamma = 2.1$) and axial compression (shortening ~50%) at 800°C, a shear strain rate of 10⁻⁵/sec and 1200 MPa (regime 2). The shear zone boundaries are parallel to the horizontal edges of the photo; shearing was sinistral. Note that the recrystallized grains, which result from progressive subgrain misorientation, define a foliation which is oblique to the shear plane (and which does not change in angle with progressive strain). (W432)

Experimentally deformed quartz aggregates

Figure caption

Experimentally deformed quartz aggregates

starting materials / semi-brittle & regime 1 / regime 2 / regime 2 & 3 / annealing

8



BHQ shortened 30% at 900°C, 10⁻⁶/sec and 1200 MPa ('wet'); transition between regime 2-3 dislocation creep.

BHQ shortened ~30% at 900°C, 10⁻⁶/sec and 1200 MPa, with ~0.2 wt % water added. Deformation occurred in the transition region between regime 2 and regime 3 dislocation creep. Recovery occurs by dislocation climb, thus subgrains form within original grains. All grain boundaries are very mobile at this temperature, despite the low driving force (e.g., low dislocation density contrast), thus there is a greater extent of dynamic recrystallization at low sample strain than is the case for regime 2 dislocation creep. (CQ78)

Experimentally deformed quartz aggregates

Figure caption

Experimentally deformed quartz aggregates

starting materials / semi-brittle & regime 1 / regime 2 / regime 2 & 3 / annealing

9



BHQ shortened ~ 40% at 900°C, 10⁻⁶/sec and 1200 MPa ('wet'); transition between regime 2 - 3 dislocation creep.

BHQ shortened 40% at 900°C, 10⁻⁶/sec and 1200 MPa, with ~0.2 wt % water added. This photo shows a higher strain portion of the same sample illustrated in #8. The original grains are not visibly flattened but have been about half consumed by relatively large dynamically recrystallized grains. Subgrains are present within original grains, but deformation lamellae are rare. In regime 3 the recrystallized grains tend to be substantially larger than the subgrains within original grains, again due to high grain boundary mobility. (CQ78)

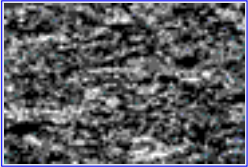
Experimentally deformed quartz aggregates

Figure caption

Experimentally deformed quartz aggregates

starting materials / semi-brittle & regime 1 / regime 2 / regime 2 & 3 / annealing

10



BHQ shortened 57% at 900°C, 10⁻⁶/sec and 1200 MPa ('wet'); transition between regime 2 - 3 dislocation creep.

BHQ shortened 57% at 900°C, 10⁻⁶/sec and 1200 MPa, with ~0.2 wt % water added. This sample is ~80-90% recrystallized, with only a slight indication of flattening of original grains. This sample exhibited steady state flow (constant flow stress), and was quenched from experimental conditions. Dynamic recrystallization produced a decrease in grain size to a steady state value (6-8 μm); thus the recrystallized grain size should reflect only the stress magnitude. (CQ82)

Experimentally deformed quartz aggregates

Figure caption

Experimentally deformed quartz aggregates

starting materials / semi-brittle & regime 1 / regime 2 / regime 2 & 3 / annealing

11



Arkansas novaculite (original $d = 5 \mu\text{m}$) shortened 54% at 900°C , 10-6/sec and 1200 MPa ('wet'); transition between regime 2 - 3 dislocation creep.

Arkansas novaculite with an original grain size of $5 \mu\text{m}$ which has been shortened 54% at 900°C , 10-6/sec and 1200 MPa, with ~0.2 wt % water added. This sample had the same steady state flow stress as the quartzite in photo #10; in this case dynamic recrystallization has involved an increase in grain size to essentially the same size developed in the quartzite. (CQ84)

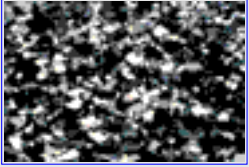
Experimentally deformed quartz aggregates

Figure caption

[Experimentally deformed quartz aggregates](#)

[starting materials](#) / [semi-brittle & regime 1](#) / [regime 2](#) / [regime 2 & 3](#) / [annealing](#)

12



BHQ shortened 50% at 1200°C, 10⁻⁶/sec and 1200 MPa; regime 3 dislocation creep.

BHQ shortened 50% at 1200°C, 10⁻⁶/sec and 1200 MPa, in regime 3 dislocation creep. This sample has been completely dynamically recrystallized, to form relatively large polygonal grains which might at first appear 'annealed' (compare with photo #14). The higher the temperature of deformation, the more closely the rate of recovery can match the rate of deformation. (W857)

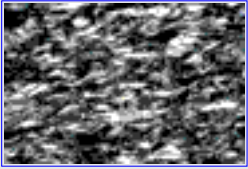
Experimentally deformed quartz aggregates

Figure caption

[Experimentally deformed quartz aggregates](#)

[starting materials](#) / [semi-brittle & regime 1](#) / [regime 2](#) / [regime 2 & 3](#) / [annealing](#)

13



BHQ shortened 60% at 800°C, 10⁻⁶/sec and 1200 MPa; regime 2 dislocation creep.

BHQ shortened 60% at 800°C, 10⁻⁶/sec and 1200 MPa (regime 2). Same features as described for photo #6. Compare this photo with photo #14, which shows a sample that was deformed at identical conditions but then statically annealed. (AN8)

Experimentally deformed quartz aggregates

Figure caption

Experimentally deformed quartz aggregates

starting materials / semi-brittle & regime 1 / regime 2 / regime 2 & 3 / annealing

14



BHQ shortened 60% at 800°C, 10⁻⁶/sec and 1200 MPa (regime 2 dislocation creep); then annealed at 900°C for 120 hrs.

BHQ shortened 60% at 800°C, 10⁻⁶/sec and 1200 MPa (regime 2) and then statically annealed at 900°C for 120 hours. The deformation microstructure has been completely replaced by strain-free polygonal recrystallized grains, but the pattern and the strength of the c-axis crystallographic preferred orientation has not changed. Compare this photo with #12, which shows a sample dynamically recrystallized at high temperature; in the annealed sample the grain boundaries are straighter, but both samples were quenched. Would differences be preserved and noticeable in naturally deformed (and possibly annealed) samples? (AN9)

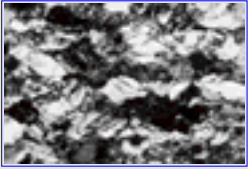
Experimentally deformed quartz aggregates

Figure caption

Experimentally deformed quartz aggregates

starting materials / semi-brittle & regime 1 / regime 2 / regime 2 & 3 / annealing

21



HQ, shortened 50% at 700°C, 10⁻⁵/sec and 1200 MPa, in the semi-brittle flow regime

The temperature is too low for either dislocation climb or grain boundary bulging recrystallization. Gliding dislocations rapidly tangle, creating high density tangles and thus strain hardening. Eventually the stress becomes high enough to nucleate cracks. The combination of distributed dislocations plus microcracks produces extremely strong and patchy undulatory extinction in most grains. In addition many grains develop multiple grain-scale faults, marked by strong narrow deformation bands and grain boundary offsets. (CQ10)

2

Naturally deformed quartz-rich rocks

TOP

- | | |
|---|--|
| <u>1-</u> Experimentally deformed quartz aggregates | <u>2-</u> Naturally deformed quartz-rich rocks |
| <u>3-</u> Experimentally deformed feldspar aggregates | <u>4-</u> Naturally deformed feldspar rocks |
| <u>5-</u> Experimentally deformed quartzo-feldspathic rocks | <u>6-</u> Naturally deformed quartzo-feldspathic rocks |
| <u>7-</u> Experimentally deformed pyroxenite and diabase | <u>8-</u> Deformation and metamorphic reactions in polyphase rocks |

Naturally deformed quartz-rich rocks

undeformed / semibrittle & bulging recrystallization / subgrain rotation recrystallization / grain boundary migration recrystallization

Introduction

In naturally deformed quartz-rich rocks, the microstructures show systematic differences with increasing temperatures of deformation, similar to the different dislocation creep regimes in experimentally deformed examples. The strain rate and stress conditions of the naturally deformed rocks usually are unknown or poorly constrained, so that a direct correlation with dislocation creep regimes could be difficult. However, the dominant recrystallization mechanisms can be determined from the microstructures and can be compared with the experimentally established dislocation creep regimes. Three microstructural regimes corresponding to three main mechanisms of dynamic recrystallization can be distinguished:

1. Bulging recrystallization which is dominated by local grain boundary migration (slow migration) and occurs at the lowest temperatures of deformation. The grain boundary lobes are very small. Favorite sites for bulging are triple junctions, and - if present - fractures.
2. Progressive subgrain rotation which is dominated by polygonization of old grains and formation of newly recrystallized grains. This recrystallization occurs at intermediate temperatures.
3. Grain boundary migration recrystallization which is dominated by fast grain boundary migration and occurs at high temperatures. During this recrystallization, whole grains may be swept. Progressive subgrain rotation is only important for the initial formation of new grains.

Generally, the recrystallization mechanisms listed above as 1,2,3

correspond approximately to the dominant recrystallization processes identified in the respective experimental dislocation creep regimes 1,2,3.

The Heavitree quartzite is from the Ruby Gap duplex (RGD) which forms a part of the internal ductile zones of the Alice Springs orogen in central Australia. The RGD consists of 5 thrust sheets of Heavitree quartzite deformed under greenschist-facies conditions (less than 400°C). Sheets 1, 2 and 3 form an imbricate system. Finite strain and temperature of deformation generally increase upward through the duplex. The microstructures are typical of the full spectrum of dislocation creep regimes.

The chert samples are from the Warrawoona syncline which is part of an Archean greenstone belt accumulated between 3450 Ma and 3320 Ma. The syncline is a tight keel structure developed between two granitic domes. In the axis of the syncline, a chert series was deformed and recrystallized under greenschist-facies conditions. The tectonites are very strongly lineated in the central part of the syncline, and shape and crystallographic fabric analyses indicate a deformation in constriction. During deformation-recrystallization, the chert underwent substantial grain growth.

The quartz veins are from the Tonale Line, a major strike slip fault in the Alps. At the eastern end, the synkinematic Adamello intrusion has imposed a thermal gradient across the fault. The quartz samples shown here come from the Edolo shists which were deformed under greenschist-facies conditions.

[further reading](#)

Naturally deformed quartz-rich rocks

Further reading

Naturally deformed quartz-rich rocks undeformed / semi-brittle & bulging recrystallization / subgrain rotation recrystallization / grain boundary migration recrystallization

Dunlap, W.J., Hirth, G. and Teyssier, C., 1997, Thermomechanical evolution of a ductile duplex. *Tectonics*, 16, 983-1000.

Hirth, G., Teyssier, C. and Dunlap, W.J., An evaluation of quartzite flow laws based on comparisons between experimentally and naturally deformed rocks, In press, *Geol. Rundsch.*

van Daalen, M., Heilbronner, R. & Kunze, K. 1999. Orientation analysis of localized shear deformation in quartz fibres at the brittle&endash;ductile transition. *Tectonophysics* 303, 83-108.

Pauli, C., Schmid, S. M. & Panozzo Heilbronner, R. 1996. Fabric domains in quartz mylonites: localized three dimensional analysis of microstructure and texture. *J. Structural Geology* 18, 1183-1203.

Naturally deformed quartz-rich rocks

Semibrittle behaviour & bulging recrystallization

Naturally deformed quartz-rich rocks

undeformed / semibrittle & bulging recrystallization / subgrain rotation recrystallization / grain boundary migration recrystallization

List of microstructures

15



[Semi-brittle deformation of quartz vein, Eastern Tonale line.](#)

16



[Bulging recrystallization of quartz vein, Eastern Tonale line.](#)

Naturally deformed quartz-rich rocks

Subgrain rotation recrystallization

Naturally deformed quartz-rich rocks

undeformed / semibrittle & bulging recrystallization / subgrain rotation recrystallization / grain boundary migration recrystallization

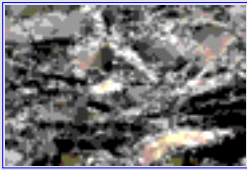
List of microstructures

18



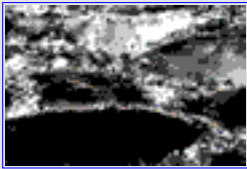
Mica-rich Heavitree quartzite deformed at greenschist conditions by simultaneous subgrain rotation recrystallization and solution-reprecipitation

19



Mica-poor Heavitree quartzite deformed at greenschist conditions by subgrain rotation recrystallization.

20



Detail of mica-poor Heavitree quartzite, showing recrystallization by progressive subgrain misorientation.

Naturally deformed quartz-rich rocks

Undeformed

Naturally deformed quartz-rich rocks

undeformed / semibrittle & bulging recrystallization / subgrain rotation recrystallization / grain boundary migration recrystallization

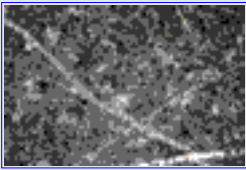
List of microstructures

17



Relatively undeformed Heavitree quartzite containing some fine-grained mica.

26



Undeformed chert, with patches of different grain sizes and quartz veins.

Naturally deformed quartz-rich rocks

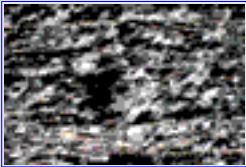
Grain boundary migration recrystallization

Naturally deformed quartz-rich rocks

undeformed / semibrittle & bulging recrystallization / subgrain rotation recrystallization / grain boundary migration recrystallization

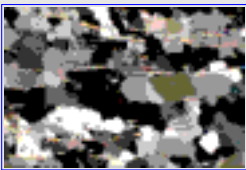
List of microstructures

22



Mica-rich Heavitree quartzite showing by grain boundary migration recrystallization; mica grains pin the boundaries of recrystallized quartz grains.

25



Less micaceous Heavitree quartzite; note larger, equant recrystallized grains.

27



Chert deformed and recrystallized at greenschist conditions; grain growth was greater in pure quartz regions.

28



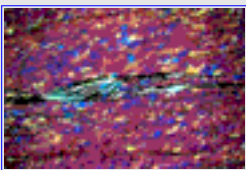
Chert deformed at greenschist conditions, showing that dynamic recrystallization can produce an increase in grain size.

29



Chert deformed and recrystallized at greenschist conditions. Grain size depends on purity; coarser grain size region represents quartz veins.

30



Mica fish and oblique elongate recrystallized quartz grains in quartz mylonite, indicating dextral shear.

Naturally deformed quartz-rich rocks

Figure caption

Naturally deformed quartz-rich rocks

undeformed / semibrittle & bulging recrystallization / subgrain rotation recrystallization / grain boundary migration recrystallization

15



Semi-brittle deformation of quartz vein, Eastern Tonale line.

Sample is from the cataclastic fault zone; deformation conditions are approximately 260°C, 200-300 MPa. Deformation is mainly by fracturing as evidenced by offsets along grain boundaries. Quartz grains show undulose and patchy extinction. Small scale serration of grain boundaries and very small recrystallized grains of the same size as the bulges indicate incipient dynamic recrystallization by bulging recrystallization. New grains form predominantly along fractures and at crack tips. (MS76-3)

Naturally deformed quartz-rich rocks

Figure caption

Naturally deformed quartz-rich rocks

undeformed / semibrittle & bulging recrystallization / subgrain rotation recrystallization / grain boundary migration recrystallization

16



Bulging recrystallization of quartz vein, Eastern Tonale line.

Sample is from the mylonitic fault zone; deformation conditions are approximately 340°C, 200-300 MPa. Quartz grains show undulose and patchy extinction; the grain boundaries are clearly serrated indicating bulging recrystallization. The recrystallized new grains at the rims of the porphyroclasts occur more extensively at triple junctions and along grain boundaries that are oriented at high angles to the foliation. Apparent flattening and stretching of porphyroclasts is partly due to initially elongated shape of quartz fibres. Larger irregular subgrains are probably not synkinematic. (MS26-2)

Naturally deformed quartz-rich rocks

Figure caption

Naturally deformed quartz-rich rocks

undeformed / semibrittle & bulging recrystallization / subgrain rotation recrystallization / grain boundary migration recrystallization

17



Relatively undeformed Heavitree quartzite containing some fine-grained mica.

Relatively undeformed Heavitree Quartzite of Sheet 1. Weak foliation oriented NE-SW defined by fine micas grown in the pressure shadows of quartz grains. Some quartz grains consist of a detrital grain over which quartz cement has grown in the same crystallographic orientation. (59 A)

Naturally deformed quartz-rich rocks

Figure caption

Naturally deformed quartz-rich rocks

undeformed / semibrittle & bulging recrystallization / subgrain rotation recrystallization / grain boundary migration / recrystallization

18



Mica-rich Heavitree quartzite deformed at greenschist conditions by simultaneous subgrain rotation recrystallization and solution-reprecipitation.

In mica-rich quartzite of sheet 2, detrital quartz grains are flattened, stretched, and bent in a fine-grained quartz-mica matrix. Some quartz grains have undergone dissolution on ~E-W oriented grain boundaries but others have bent and flattened by regime 2 dislocation creep. A NE-SW shear band deforms the dominant foliation and indicates top-to-the-left sense of shear. (704 A)

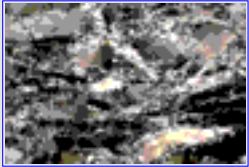
Naturally deformed quartz-rich rocks

Figure caption

Naturally deformed quartz-rich rocks

undeformed / semibrittle & bulging recrystallization / subgrain rotation recrystallization / grain boundary migration / recrystallization

19



Mica-poor Heavitree quartzite deformed at greenschist conditions by subgrain rotation recrystallization.

In mica-poor quartzites of sheet 2, deformed at same conditions as sample shown in photo #18, there is little or no solution-precipitation. Original detrital quartz grains are flattened and stretched and show severe undulose extinction due to the development of subgrains by lattice rotation. The large grains are surrounded by a mantle of recrystallized grains, ~50 μm in size, which formed by subgrain rotation in dislocation creep regime 2. The recrystallized grains are larger than in the sample illustration in photo 18 because the grain boundaries were not pinned by micas. (703 A)

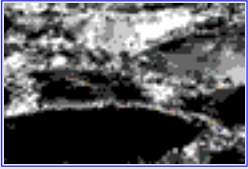
Naturally deformed quartz-rich rocks

Figure caption

Naturally deformed quartz-rich rocks

undeformed / semibrittle & bulging recrystallization / subgrain rotation recrystallization / grain boundary migration recrystallization

20



Detail of mica-poor Heavitree quartzite, showing recrystallization by progressive subgrain misorientation.

Detail of photo #19. Original grains contain subgrains that grade into recrystallized grains toward their margins or in linear zones that may have originated as fractures or deformation bands. The similarity in shape and size of low-angle subgrains and high-angle recrystallized grains suggests that progressive rotation was the dominant process of dynamic recrystallization (dislocation creep regime 2). (703 A)

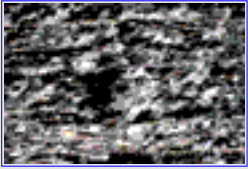
Naturally deformed quartz-rich rocks

Figure caption

Naturally deformed quartz-rich rocks

undeformed / semibrittle & bulging recrystallization / subgrain rotation recrystallization / grain boundary migration recrystallization

22



Mica-rich Heavitree quartzite showing grain boundary migration recrystallization; mica grains pin the boundaries of recrystallized quartz grains.

In this sample, the quartz recrystallized grain size is limited by mica grains pinning the grain boundaries; in mica-poor layers, the quartz recrystallized grain size is larger. Dislocation creep regime 3. (SI-11 A)

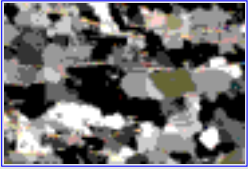
Naturally deformed quartz-rich rocks

Figure caption

Naturally
deformed
quartz-rich rocks

undeformed / semibrittle & bulging recrystallization / subgrain rotation recrystallization / grain boundary migration
recrystallization

25



Less micaceous Heavitree quartzite; note larger, equant recrystallized grains.

The recrystallized grain size is limited by the larger mica grains, although quartz boundaries were able to migrate past smaller mica grains. The distribution of small micas might indicate the characteristic recrystallized grain size at an earlier stage of the deformation-recrystallization. Dislocation creep regime 3. (249 A)

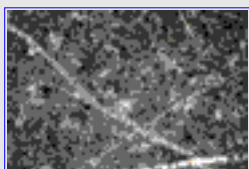
Naturally deformed quartz-rich rocks

Figure caption

Naturally deformed quartz-rich rocks

undeformed / semibrittle & bulging recrystallization / subgrain rotation recrystallization / grain boundary migration recrystallization

26



Undeformed chert, with patches of different grain sizes and quartz veins.

Undeformed chert at Marble Bar, Pilbara, Western Australia. Several generations of quartz veins crosscut the chert. The chert includes patches with different grain sizes of quartz. (76)

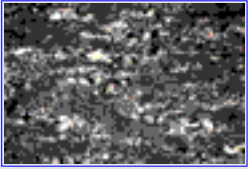
Naturally deformed quartz-rich rocks

Figure caption

Naturally deformed quartz-rich rocks

undeformed / semibrittle & bulging recrystallization / subgrain rotation recrystallization / grain boundary migration recrystallization

27



Chert deformed and recrystallized at greenschist conditions; grain growth was greater in pure quartz regions.

Chert from Pilbara, Western Australia, deformed at greenschist conditions. The patchiness of quartz grain sizes persists through the early stages of deformation and dynamic recrystallization, and is enhanced by the greater grain growth in regions of more pure quartz. (110)

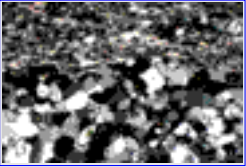
Naturally deformed quartz-rich rocks

Figure caption

Naturally deformed quartz-rich rocks

undeformed / semibrittle & bulging recrystallization / subgrain rotation recrystallization / grain boundary migration recrystallization

28



Chert deformed at greenschist conditions, showing that dynamic recrystallization can produce an increase in grain size.

Chert from Pilbara, Western Australia, deformed at greenschist conditions. Dynamic recrystallization has resulted in coarsening of the quartz grain size. The foliation is defined by the alternation of recrystallized chert and transposed and recrystallized quartz veins (largest grain sizes). White mica pins the quartz boundaries in the chert, but in the layers of large quartz grain size, micas are contained within individual quartz grains. These microstructural relations indicate grain boundary migration in dislocation creep regime 3. (606 A)

Naturally deformed quartz-rich rocks

Figure caption

Naturally deformed quartz-rich rocks

undeformed / semibrittle & bulging recrystallization / subgrain rotation recrystallization / grain boundary migration recrystallization

29



Chert deformed and recrystallized at greenschist conditions. Grain size depends on purity; coarser grain size regions represent quartz veins.

Chert from Pilbara, Western Australia, deformed at greenschist conditions. Very strong macroscopic foliation and lineation. Grain size coarsening is a function of quartz purity, the quartz veins showing the largest grain size. Recrystallized quartz grains are elongate oblique to the main foliation, in a manner consistent with top-to-the-left sense of shear. Deformation occurs in transition between regime 2 and 3 dislocation creep. (119 A)

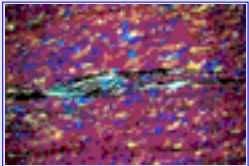
Naturally deformed quartz-rich rocks

Figure caption

Naturally deformed quartz-rich rocks

undeformed / semibrittle & bulging recrystallization / subgrain rotation recrystallization / grain boundary migration recrystallization

30



Mica fish and oblique elongate recrystallized quartz grains in quartz mylonite, indicating dextral shear.

Mica fish in quartzite mylonite, Redbank shear zone, central Australia, deformed at greenschist conditions. Gypsum plate inserted shows strong crystallographic preferred orientation as well as oblique foliation of elongate recrystallized quartz grains consistent with the top-to-the-right (south) sense of shear inferred from mica fish. The section is perpendicular to foliation and parallel to lineation; most c-axes lie in the foliation and are normal to lineation (red-purple grains) and a few define a part of a cross-girdle (blue and yellow grains). (428 A)

3

Experimentally deformed feldspar aggregates

TOP

- | | |
|---|--|
| <u>1-</u> Experimentally deformed quartz aggregates | <u>2-</u> Naturally deformed quartz-rich rocks |
| <u>3-</u> Experimentally deformed feldspar aggregates | <u>4-</u> Naturally deformed feldspar rocks |
| <u>5-</u> Experimentally deformed quartzo-feldspathic rocks | <u>6-</u> Naturally deformed quartzo-feldspathic rocks |
| <u>7-</u> Experimentally deformed pyroxenite and diabase | <u>8-</u> Deformation and metamorphic reactions in polyphase rocks |

Experimentally deformed feldspar aggregates

Starting material / cataclastic flow / regime 1

Introduction

The photos in this chapter illustrate the full transition from brittle faulting to macroscopically ductile cataclastic flow (distributed microcracking and grain-scale faulting) to crystal plasticity (crack-free dislocation creep), which occurs with increasing temperature and pressure. The field of cataclastic flow is especially well developed in feldspar aggregates (it does not occur at all in quartz aggregates), due to the two excellent cleavages in this mineral. One photo illustrates the effects of previous brittle faulting on later high temperature deformation. Although there is evidence from naturally deformed rocks that feldspars show the same 3 dislocation creep regimes as quartz, characterized by distinct mechanisms of dynamic recrystallization, so far we have only been able to achieve the lowest temperature 'regime 1' in laboratory experiments, before being cut off by melting. Thus that is the only type of dislocation creep microstructure illustrated in this chapter; for microstructures characteristic of higher temperature regimes, see Chapter 4 (Naturally Deformed Feldspar Rocks).

It is important to mention that in nature, the deformation of feldspars at conditions appropriate for the low temperature 'regime 1' dislocation creep almost always involves the additional complexity of chemical change. Recent experiments have been done to investigate the microstructures produced in such cases, but they are not included here; for natural examples, see Chapter 8 (Deformation and Metamorphic Reactions in Polyphase Rocks).

All of the samples illustrated in this chapter have been deformed in axial compression, at constant strain rate, but several photos illustrate

the microstructures developed under shear, which occurs around the corners of the top piston as it moves down into the sample at high strain.

[further reading](#)

Experimentally deformed feldspar aggregates

Further reading

Experimentally deformed feldspar aggregates

Starting material / cataclastic flow / regime 1

Post, A.D. and Tullis, J., 1999, A recrystallized grain size piezometer for experimentally deformed feldspar aggregates. *Tectonophys.*, 303, 159-173.

Tullis, J. and Yund, R.A., 1987, Transition from cataclastic flow to dislocation creep of feldspar: mechanisms and microstructures: *Geology*, 15, 606-609.

Tullis, J., and Yund, R.A., 1992, The brittle-ductile transition in feldspar aggregates: an experimental study: in, *Fault Mechanics and Transport Properties of Rocks*, B. Evans & T.-f. Wong, eds., Academic Press, NY, 89-118.

Tullis, J. and Yund, R.A., 1985, Dynamic recrystallization of feldspar: a mechanism for ductile shear zone formation: *Geology*, 13, 238-241.

Tullis, J., Dell'Angelo, L.N., and Yund, R.A., 1990, Ductile shear zones from brittle precursors in feldspathic rocks; the possible role of dynamic recrystallization: in *The Brittle-Ductile Transition: The Heard Volume*, A. Duba, W. Durham, J. Handin, and H. Wang, eds., , Amer. Geophys. Union Monograph 56, 67-82.

Yund, R.A., and Tullis, J., 1991, Compositional changes of minerals associated with dynamic recrystallization. *Contrib. Mineral. Petrol.*, 108, 346-355.

Experimentally deformed feldspar aggregates

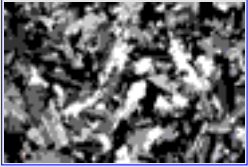
Starting material

Experimentally deformed feldspar aggregates

[Starting material](#) / [cataclastic flow](#) / [regime 1](#)

List of microstructures

31



[Tanco albite \(TA\) starting material \(An1\).](#)

41



[Bushveld anorthosite \(BA\) starting material \(An78\).](#)

44



[Hale albite \(HA\) starting material \(An1\).](#)

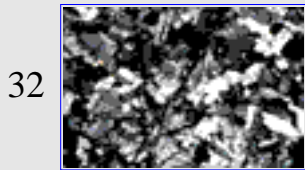
Experimentally deformed feldspar aggregates

Cataclastic flow

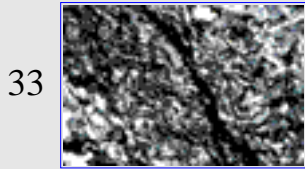
Experimentally deformed feldspar aggregates

[Starting material](#) / [cataclastic flow](#) / [regime 1](#)

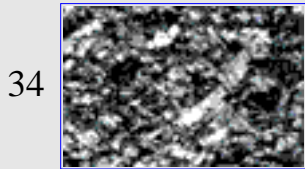
List of microstructures



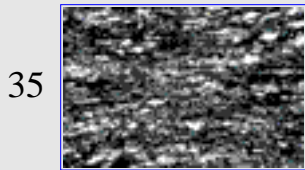
[TA shortened 15% at 20°C, 10⁻⁵/sec, and 800 MPa; brittle fault with stress drop.](#)



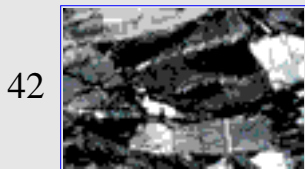
[TA shortened 35% at 200°C, 10⁻⁵/sec, and 800 MPa; wider zone of comminution with no stress drop.](#)



[TA shortened 34% at 300°C, 10⁻⁵/sec, and 800 MPa; macroscopically ductile cataclastic flow.](#)



[TA shortened 50% at 800°C, 10⁻⁵/sec, and 1200 MPa; semi-brittle flow.](#)



[BA shortened 31% at 300°C, 10⁻⁵/sec, and 800 MPa; macroscopically ductile cataclastic flow.](#)



[BA shortened 23% at 350°C, 10⁻⁵/sec, and 800 MPa; dextral shear by cataclastic flow.](#)

Experimentally deformed feldspar aggregates

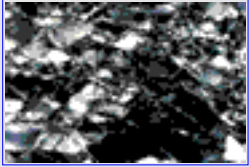
Regime 1

Experimentally deformed feldspar aggregates

[Starting material](#) / [cataclastic flow](#) / [regime 1](#)

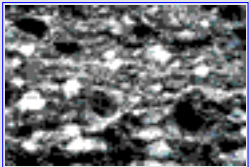
List of microstructures

45



[HA shortened 56% at 1000°C, 10⁻⁶/sec, and 1200 MPa; regime 1 dislocation creep.](#)

46



[HA shortened 70% at 1100°C, 10⁻⁶/sec, and 1200 MPa; regime 1 dislocation creep.](#)

36



[TA shortened 52% at 1100°C, 10⁻⁵/sec, and 1200 MPa; regime 1 dislocation creep.](#)

37



[TA shortened 35% at 900°C, 10⁻⁶/sec, and 1200 MPa; localized dextral shear zone has formed due to regime 1 dislocation creep.](#)

38



[TA shortened 35% at 900°C, 10⁻⁶/sec, and 1200 MPa; narrow zones of very fine recrystallized grains \(regime 1 dislocation creep\) allow localized dextral shear.](#)

39



[TA pre-faulted at low P and T, then shortened 30% at 900°C, 10⁻⁶/sec, and 1200 MPa; regime 1 dislocation creep localized along former fault.](#)

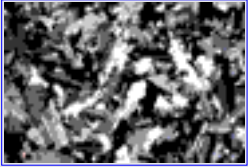
Experimentally deformed feldspar aggregates

Figure caption

Experimentally
deformed
feldspar
aggregates

Starting material / cataclastic flow / regime 1

31



Tanco albite (TA) starting material (An1).

Tanco albite (TA) starting material. Very pure albite (An1) aggregate (~1% apatite and trace of muscovite) from border zone of Tanco pegmatite, Ontario. Average grain size ~200 μm ; most grains contain growth twins. In some blocks of this material the lath-shaped grains are randomly oriented whereas in others they are quite strongly aligned.

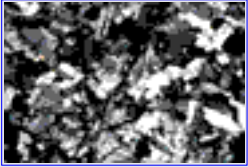
Experimentally deformed feldspar aggregates

Figure caption

Experimentally
deformed
feldspar
aggregates

Starting material / cataclastic flow / regime 1

32



TA shortened 15% at 20°C, 10-5/sec, and 800 MPa; brittle fault with stress drop.

TA shortened 15% at 20°C, 10-5/sec, 800 MPa. Sample underwent brittle failure (seismic, with sudden stress drop) along a fault at ~ 30° to σ_1 which formed from the coalescence of axial (mode I) cracks. The fine-grained fault gouge appears black. (W546)

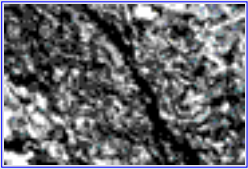
Experimentally deformed feldspar aggregates

Figure caption

Experimentally
deformed
feldspar
aggregates

Starting material / cataclastic flow / regime 1

33



TA shortened 35% at 200°C, 10-5/sec, and 800 MPa; wider zone of comminution with no stress drop.

TA shortened 35% at 200°C, 10-5/sec, 800 MPa. Sample shows a discrete fault plane but a wide zone on either side of distributed cracking and multiple grain-scale faulting. This sample did not have a sudden stress drop. (W530)

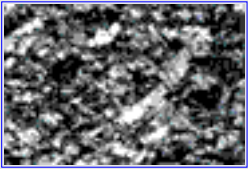
Experimentally deformed feldspar aggregates

Figure caption

Experimentally
deformed
feldspar
aggregates

Starting material / cataclastic flow / regime 1

34



TA shortened 34% at 300°C, 10⁻⁵/sec, and 800 MPa; macroscopically ductile cataclastic flow.

TA shortened 34% at 300°C, 10⁻⁵/sec, 800 MPa. The deformation of this sample is macroscopically ductile although microscopically brittle, because there has been no dislocation activity or even mechanical twinning (determined by TEM observations). Cracking remained distributed, instead of coalescing into a through-going fault, and the sample underwent close to steady state flow. We have termed this 'cataclastic flow'. Most grains show multiple grain-scale faulting, most commonly on one or both cleavage planes. (W528)

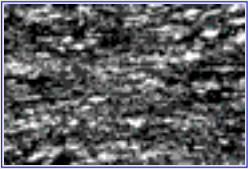
Experimentally deformed feldspar aggregates

Figure caption

Experimentally
deformed
feldspar
aggregates

Starting material / cataclastic flow / regime 1

35



TA shortened 50% at 800°C, 10⁻⁵/sec, and 1200 MPa; semi-brittle flow.

TA shortened 50% at 800°C, 10⁻⁵/sec, 1200 MPa. This sample deformed by semi-brittle flow; TEM shows that there was limited dislocation glide, but no recovery or recrystallization, and thus extreme work hardening resulted in distributed microcracking. This sample demonstrates that multiple grain-scale faulting can produce a grain shape foliation. (W447)

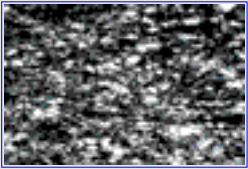
Experimentally deformed feldspar aggregates

Figure caption

Experimentally
deformed
feldspar
aggregates

Starting material / cataclastic flow / regime 1

36



TA shortened 52% at 1100°C, 10⁻⁵/sec, and 1200 MPa; regime 1 dislocation creep.

TA shortened 52% at 1100°C, 10⁻⁵/sec, 1200 MPa. This sample was deformed in the lower temperature dislocation creep regime (regime 1 of Hirth & Tullis, 1992). The temperature is not high enough to activate dislocation climb and thus grain boundary migration recrystallization serves as the recovery process. Original grains undergo relatively little and very inhomogeneous strain; they develop strong patchy undulatory extinction and sharp deformation bands or even several grain-scale faults, which together with the original grain boundaries develop zones of extremely fine ($d \sim 1 \mu\text{m}$) recrystallized grains along them. The recrystallized grains are initially strain-free and thus significantly weaker than the larger work-hardened original grains, and thus strain is preferentially partitioned into the recrystallized zones. This photo shows that original grains have been separated into several smaller lozenge-shaped grains, and there are thin zones of extremely fine recrystallized grains along all of the original and the new grain boundaries. The sample had a relatively high yield strength, followed by strain weakening which began when an interconnected network of recrystallized grains developed. Compare the microstructure of this sample with that shown in photo #35, which was produced by cataclastic flow. (W561)

Experimentally deformed feldspar aggregates

Figure caption

Experimentally
deformed
feldspar
aggregates

Starting material / cataclastic flow / regime 1

37



TA shortened 35% at 900°C, 10⁻⁶/sec, and 1200 MPa; localized dextral shear zone has formed due to regime 1 dislocation creep.

TA shortened 35% at 900°C, 10⁻⁶/sec, 1200 MPa. In this sample the starting material had well-aligned laths, which were oriented parallel to the sample core axis and thus parallel to compression. During the deformation the sample buckled; the original foliation is almost vertical in the lower left corner, curves around to the right, and then becomes vertical again in the upper right corner. Very thin dextral shear zones of (regime 1) dynamically recrystallized grains have developed (NW-SE) and are accommodating almost all of the further sample strain. (W694)

Experimentally deformed feldspar aggregates

Figure caption

Experimentally
deformed
feldspar
aggregates

Starting material / cataclastic flow / regime 1

38



TA shortened 35% at 900°C, 10⁻⁶/sec, and 1200 MPa; narrow zones of very fine recrystallized grains (regime 1 dislocation creep) allow localized dextral shear.

Higher magnification view of a portion of the shear zone region in the sample shown in photo #37. The recrystallized grains within the thin dextral shear zones are only ~1 μm in diameter; because they are so small, grain boundary migration can frequently sweep through them and remove any accumulated dislocations. The faster recovery in the fine grained zones makes them weaker and causes strain to be strongly localized. (W694)

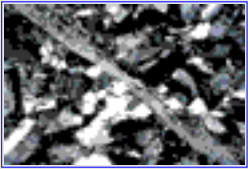
Experimentally deformed feldspar aggregates

Figure caption

Experimentally
deformed
feldspar
aggregates

Starting material / cataclastic flow / regime 1

39



TA pre-faulted at low P and T, then shortened 30% at 900°C, 10⁻⁶/sec, and 1200 MPa; regime 1 dislocation creep localized along former fault.

TA pre-faulted at 300°C, 10⁻⁴/sec, 400 MPa and then taken to 900°C and 1200 MPa and shortened 30% at 10⁻⁶/sec. The high temperature deformation has been almost entirely partitioned into the pre-existing thin zone of finer grain size. The fine-grained zone was able to rapidly undergo complete dynamic recrystallization (by the low T grain boundary migration mechanism), and then was significantly weaker than the coarser-grained material on either side. This is one process by which ductile shear zones may form. The fine-grained albite within the shear zone has in a general sense undergone 'superplastic flow' but the process was not predominantly grain boundary sliding with diffusion creep, as inferred from the strong crystallographic preferred orientation and the high dislocation densities observed in TEM. (W485)

Experimentally deformed feldspar aggregates

Figure caption

Experimentally
deformed
feldspar
aggregates

Starting material / cataclastic flow / regime 1

41



Bushveld anorthosite (BA) starting material (An78).

Bushveld anorthosite (BA) starting material, from South Africa. The composition is An78 and the average grain size is ~300-400 μm . Most grains contain albite twins. There is a small amount of sericitic alteration, and small pyroxene grains are present in some sections.

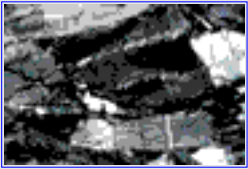
Experimentally deformed feldspar aggregates

Figure caption

Experimentally
deformed
feldspar
aggregates

Starting material / cataclastic flow / regime 1

42



BA shortened 31% at 300°C, 10⁻⁵/sec, and 800 MPa; macroscopically ductile cataclastic flow.

BA shortened 31% at 300°C, 10⁻⁵/sec, 800 MPa. At these conditions there is no dislocation glide or mechanical twinning; the samples deform by distributed cracking, including multiple grain-scale faulting, and thus are macroscopically ductile. This high magnification view shows multiple grain-scale faults, beautifully revealed by offset of original twins. In many but not all cases the grain-scale faults are developed along cleavage planes. (CF39)

Experimentally deformed feldspar aggregates

Figure caption

Experimentally
deformed
feldspar
aggregates

Starting material / cataclastic flow / regime 1

43



BA shortened 23% at 350°C, 10⁻⁵/sec, and 800 MPa; dextral shear by cataclastic flow.

BA shortened 23% at 350°C, 10⁻⁵/sec, 800 MPa. This view shows a corner of a sample where there has been overall dextral shear around the piston edge, and illustrates how multiple grain-scale faulting is able to accomplish macroscopically ductile deformation. TEM shows that the undulatory extinction visible in some grains is due to arrays of submicroscopic cracks; the deformation involved no dislocation glide. (CF12)

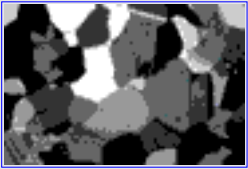
Experimentally deformed feldspar aggregates

Figure caption

Experimentally
deformed
feldspar
aggregates

Starting material / cataclastic flow / regime 1

44



Hale albite (HA) starting material (An1).

Hale albite (HA) starting material. This fine-grained albite (An1) rock comes from the border zone of the Hale pegmatite in Middletown, Connecticut. The grains are more equant than those in the Tanco albite, with an average diameter of 200 μm . Some grains contain Albite twins; there are trace amounts of muscovite and tourmaline in some sections.

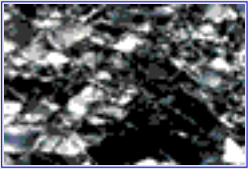
Experimentally deformed feldspar aggregates

Figure caption

Experimentally
deformed
feldspar
aggregates

Starting material / cataclastic flow / regime 1

45



HA shortened 56% at 1000°C, 10⁻⁶/sec, and 1200 MPa; regime 1 dislocation creep.

HA shortened 56% at 1000°C, 10⁻⁶/sec, 1200 MPa. This sample has deformed by low temperature dislocation creep (regime 1 of Hirth & Tullis, 1992). Dislocation climb is difficult so original grains work harden due to development of high dislocation densities; recovery occurs by bulging recrystallization (the driving force is high even though the grain boundary mobility is low). Original grains in this sample have become separated into several lozenge-shaped grains along deformation bands or grain-scale faults; these new boundaries as well as original grain boundaries have developed a zone of extremely fine (d~1 μm) recrystallized grains, which are initially strain-free and thus much weaker than the work-hardened original grains. They maintain this weakness because they are easily and continually swept by new episodes of grain boundary migration as soon as they develop a high dislocation density. (W395)

Experimentally deformed feldspar aggregates

Figure caption

Experimentally
deformed
feldspar
aggregates

Starting material / cataclastic flow / regime 1

46



HA shortened 70% at 1100°C, 10⁻⁶/sec, and 1200 MPa; regime 1 dislocation creep.

HA shortened 70% at 1100°C, 10⁻⁶/sec, 1200 MPa. This high strain sample shows that original grains are progressively reduced in size by the grain boundary recrystallization process, without showing any internal flattening strain. Remnant augen are now 'floating' in a matrix of weaker recrystallized grains. Mechanically, coarse-grained aggregates deformed in this dislocation creep regime undergo continuous strain weakening until complete recrystallization is achieved. (RD61)

TOP

- | | |
|---|--|
| <u>1-</u> Experimentally deformed quartz aggregates | <u>2-</u> Naturally deformed quartz-rich rocks |
| <u>3-</u> Experimentally deformed feldspar aggregates | <u>4-</u> Naturally deformed feldspar rocks |
| <u>5-</u> Experimentally deformed quartzo-feldspathic rocks | <u>6-</u> Naturally deformed quartzo-feldspathic rocks |
| <u>7-</u> Experimentally deformed pyroxenite and diabase | <u>8-</u> Deformation and metamorphic reactions in polyphase rocks |

Naturally deformed feldspar rocks

regime 1 / regime 2 weakly deformed / regime 2 moderately - strongly deformed

Introduction

In naturally deformed rocks, dislocation creep in feldspar is usually found above temperatures of approximately 500°C. Below these temperatures, deformation takes place by fracturing. However, this simple temperature-classification of deformation mechanisms in feldspar is complicated by the dependence of feldspar chemistry on ambient P,T-conditions and bulk rock composition. Compositional disequilibrium may be a driving force that leads to recrystallization of plagioclase under much lower temperatures than 500°C in deformed rocks. In such cases, recrystallization is syndeformational but not dynamic, because it is not driven by strain energy alone and is better termed neo-mineralisation. In order to determine the recrystallization mechanism in plagioclase one needs to compare the chemical composition of recrystallized and host grains; if the compositions are identical the process was dynamic recrystallization, but if they are different it was neo-mineralization.

Dynamic recrystallization by regime 1 dislocation creep, with no chemical change, is very rare in nature. Samples shown here are from the Corvatsch shear zone (Engadine, Swiss Alps). Examples of low temperature recrystallization (low to mid-greenschist facies) are shown in micrographs 23 and 24. Fracturing is the most important contribution to the deformation of plagioclase in these examples, accompanied by neo-mineralization.

With the exception of photo 47, the series of samples of regime 2 come from a shear zone between Sogndal and Kaupanger (Norway), in an anorthosite body of the Jotun nappe, which is part of the "middle allochthonous unit" of the Caledonides. The samples represent stages of progressively higher shear strain along a strain gradient from less deformed boudins into strongly deformed mylonites. Deformation

took place around 700°C at pressures below 900 MPa. The chemical composition of the recrystallized plagioclase grains is the same as that of the porphyroclasts, so that the formation of new grains represents only strain-induced dynamic recrystallization. Dynamic recrystallization took place dominantly by progressive subgrain rotation with some local grain boundary bulging (largely regime 2 dislocation creep).

[further reading](#)

Naturally deformed feldspar rocks

Further reading

Naturally deformed feldspar rocks

regime 1 / regime 2 weakly deformed / regime 2 moderately - strongly deformed

Kruse, R., and Stunitz, H., 1999, Deformation mechanisms and phase distribution in mafic high-temperature mylonites from the Jotun Nappe, southern Norway. *Tectonophys.*, 303, 223-249.

Stunitz, H., 1998, Syn-deformational recrystallization - dynamic or compositionally induced ? *Contrib. Mineral. Petrol.*, 131, 219-236.

Naturally deformed feldspar rocks

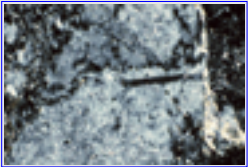
Regime 1

Naturally deformed feldspar rocks

regime 1 / regime 2 weakly deformed / regime 2 moderately - strongly deformed

List of microstructures

23



Plagioclase porphyroblast deformed under lower- to mid-greenschist facies P,T-conditions.

24



Nucleation of new grains inside fractured plagioclase porphyroblast.

Naturally deformed feldspar rocks

Regime 2 - weakly deformed

Naturally deformed feldspar rocks

regime 1 / regime 2 weakly deformed / regime 2 moderately - strongly deformed

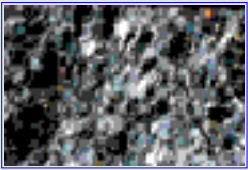
List of microstructures

47



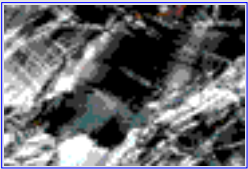
Anorthosite deformed to low strain at granulite grade, with mechanical twinning.

49



Anorthosite weakly deformed at ~700°C and 900 MPa; regime 2 dislocation creep.

50



Detail of anorthosite weakly deformed at ~700°C, 900 MPa; regime 2 dislocation creep.

Naturally deformed feldspar rocks

Regime 2 - moderately to strongly deformed

Naturally deformed feldspar rocks

regime 1 / regime 2 weakly deformed / regime 2 moderately - strongly deformed

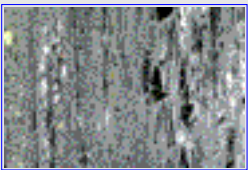
List of microstructures

51



Anorthosite moderately deformed and substantially recrystallized at ~700°C and 900 MPa; regime 2 dislocation creep.

52



Anorthosite strongly deformed and largely recrystallized at ~700°C and 900 MPa; regime 2 dislocation creep.

53



Detail of anorthosite strongly deformed and substantially recrystallized at ~700°C and 900 MPa; regime 2 dislocation creep.

54



Detail of anorthosite strongly deformed and largely recrystallized at ~700°C and 900 MPa; regime 2 dislocation creep.

Naturally deformed feldspar aggregates

Figure caption

Naturally deformed feldspar rocks

regime 1 / regime 2 low deformation / regime 2 moderate-high deformation

23



Plagioclase porphyroclast deformed under lower- to mid-greenschist facies P,T-conditions.

Below temperatures of about 500°C, feldspars tend to deform by fracturing. In the micrograph, new, fine-grained plagioclase is found along the fracture, which cuts across the grain from left to right above the twin. These new grains, however, are not formed by dynamic recrystallization in the strict sense. Instead, the new grains have a different chemical composition from that of the host grain, because intermediate plagioclase usually is metastable under greenschist facies P,T-conditions. This process constitutes a syndeformational recrystallization or neo-mineralisation. The chemical decomposition of the plagioclase porphyroclast is also evident from its "dusty" appearance, resulting from numerous solid inclusions of new phases that have nucleated. In order to decide whether the recrystallization is dynamic, i.e. driven by strain energy, or whether it is only concomitant with deformation (syndeformational) and driven by chemical disequilibrium (neo-crystallization), it is necessary to compare the chemical compositions of host and recrystallized grains. The "dusty" appearance of porphyroclasts and the presence of inclusions of mica or other phases may be an indication that the formation of new grains is due to chemical disequilibrium. See other examples in photos # 93-98. Sample is from Wyangala dam, Australia.

Naturally deformed feldspar aggregates

Figure caption

[Naturally deformed feldspar rocks](#)

[regime 1](#) / [regime 2 low deformation](#) / [regime 2 moderate-high deformation](#)

24



Nucleation of new grains inside fractured plagioclase porphyroclast.

Detail of a plagioclase porphyroclast deformed under lower- to mid-greenschist facies P,T-conditions; small new grains of a different chemical composition have nucleated (neo-mineralization). The nucleation of the new grains occurs preferentially along fractures in the host grain. Occasionally, isolated new grains appear to form inside the host grains. Fractures are usually marked by trails of fluid or solid inclusions; high magnification is required to observe such fractures. Sample is from the Corvatsch mylonite zone, Switzerland.

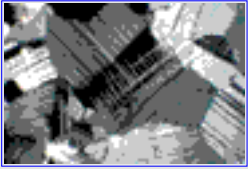
Naturally deformed feldspar aggregates

Figure caption

Naturally deformed feldspar rocks

regime 1 / regime 2 low deformation / regime 2 moderate-high deformation

47



Anorthosite deformed to low strain at granulite grade, with mechanical twinning.

Low strain anorthosite metamorphosed in the granulite facies, Ceilidh Hill, central Australia. In natural deformation of feldspars, the transition from regime 1 to regime 2 occurs at much higher temperatures than quartz, requiring at least upper amphibolite conditions. The bytownite plagioclase grains exhibit polysynthetic twins that terminate within the grains, defining them as secondary twins. (CH 1)

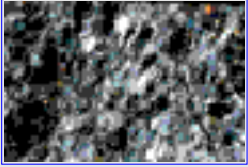
Naturally deformed feldspar aggregates

Figure caption

Naturally deformed feldspar rocks

regime 1 / regime 2 low deformation / regime 2 moderate-high deformation

49



Anorthosite weakly deformed at ~700°C and 900 MPa; regime 2 dislocation creep.

More highly deformed plagioclase from a shear zone affecting the meta-anorthosite shown in photo #47. Old plagioclase grains exhibit strong undulatory extinction and probably subgrain development. The porphyroclasts are surrounded by ~150 μm recrystallized grains that have a slightly more albitic composition. Dislocation creep regime 2. (CH 2)

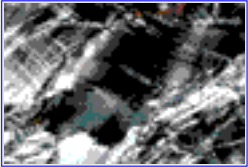
Naturally deformed feldspar aggregates

Figure caption

Naturally deformed feldspar rocks

regime 1 / regime 2 low deformation / regime 2 moderate-high deformation

50



Detail of anorthosite weakly deformed at ~700°C, 900 MPa; regime 2 dislocation creep.

Incipient recrystallization in a weakly deformed anorthosite. Core and mantle structures, resulting from subgrain rotation recrystallization, are common in many plagioclase grains. Crystal plastic deformation of plagioclase is evident from bent twin lamellae and undulose extinction. Other phases present include hornblende and garnet.

Naturally deformed feldspar aggregates

Figure caption

Naturally deformed feldspar rocks

regime 1 / regime 2 low deformation / regime 2 moderate-high deformation

51



Anorthosite moderately deformed and substantially recrystallized at ~700°C and 900 MPa; regime 2 dislocation creep.

Moderate strain anorthosite showing a porphyroblast with rectangular subgrains of a size similar to that of recrystallized matrix grains. The core-mantle structures and subgrain formation indicate that progressive subgrain rotation is the dominant mechanism of dynamic recrystallization. Some twin boundaries are recrystallized implying that twinning preceded dynamic recrystallization.

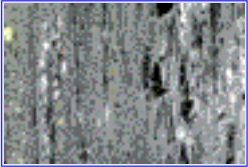
Naturally deformed feldspar aggregates

Figure caption

Naturally deformed feldspar rocks

regime 1 / regime 2 low deformation / regime 2 moderate-high deformation

52



Anorthosite strongly deformed and largely recrystallized at ~700°C and 900 MPa; regime 2 dislocation creep.

Example of strongly deformed and largely recrystallized anorthosite. Only a few porphyroclasts of plagioclase are left within a matrix of dynamically recrystallized grains. Some porphyroclasts are highly elongated, while others have lower aspect ratios. The difference in porphyroclast shapes is most likely due to the orientation of the easy slip system with respect to the shear plane and direction. Strongly elongated grains usually have their (010) planes at a small angle to the shear zone foliation and their [001] direction at a small angle to the stretching lineation. (010)[001] is one of the most important slip systems in plagioclase.

Naturally deformed feldspar aggregates

Figure caption

Naturally deformed feldspar rocks

regime 1 / regime 2 low deformation / regime 2 moderate-high deformation

53



Detail of anorthosite strongly deformed and substantially recrystallized at $\sim 700^{\circ}\text{C}$ and 900 MPa; regime 2 dislocation creep.

Higher magnification view of sample shown in photo #52, illustrating segmentation of elongated plagioclase porphyroclasts by dynamic recrystallization. Bands of recrystallized grains develop parallel to the long axes of porphyroclasts, perhaps along slip planes with higher dislocation densities, and may lead to their segmentation into narrow slivers. Thus, the aspect ratios of such slivers cannot be used to infer the total elongation of porphyroclasts.

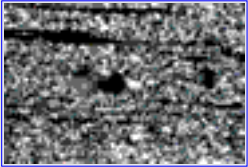
Naturally deformed feldspar aggregates

Figure caption

Naturally deformed feldspar rocks

regime 1 / regime 2 low deformation / regime 2 moderate-high deformation

54



Detail of anorthosite strongly deformed and largely recrystallized at ~700°C and 900 MPa; regime 2 dislocation creep.

Higher magnification view of sample shown in photo #52, illustrating mylonitic anorthosite. Most of the plagioclase is dynamically recrystallized and only small remnants are left of former porphyroclasts. Porphyroclasts oriented for easy slip have been reduced in thickness to the diameter of a single recrystallized grain (15-80 μm) by slip and recrystallization. Porphyroclasts with small aspect ratios have a markedly different crystallographic orientation, unsuitable for (010)[001] slip.

Experimentally deformed quartzo-feldspathic rocks

- TOP
- | | |
|---|--|
| <u>1-</u> Experimentally deformed quartz aggregates | <u>2-</u> Naturally deformed quartz-rich rocks |
| <u>3-</u> Experimentally deformed feldspar aggregates | <u>4-</u> Naturally deformed feldspar rocks |
| <u>5-</u> Experimentally deformed quartzo-feldspathic rocks | <u>6-</u> Naturally deformed quartzo-feldspathic rocks |
| <u>7-</u> Experimentally deformed pyroxenite and diabase | <u>8-</u> Deformation and metamorphic reactions in polyphase rocks |

Experimentally deformed quartzo-feldspathic rocks

starting material & regime1 / regime 2 / annealing & melting

Introduction

Most crustal rocks consist of two or more phases, which have quite different strengths or even different deformation mechanisms at a given set of conditions. Thus the strengths and microstructures in such rocks depend on the proportions as well as the arrangement of the various phases, as well as their individual flow laws. This chapter illustrates the microstructures developed in a natural fine-grained granite (aplite) deformed over a range of conditions from lower temperatures where the feldspar is semi-brittle whereas the quartz deforms by regime 1 dislocation creep, to somewhat higher temperatures where the feldspar undergoes regime 1 dislocation creep but the quartz deforms by regime 2 dislocation creep.

Most of the samples were deformed in axial compression, with strains ranging up to 85% shortening, at which point the microstructures are almost identical to some natural mylonites, with feldspar augen and quartz ribbons. The microstructures developed in simple shear are illustrated in a few photos, and the effects of static annealing following deformation are illustrated in one pair of photos.

Most of the samples were deformed at conditions where very little if any melt was involved. However, one pair of photos illustrates how a few percent melt can switch the deformation from crystal plasticity to cataclastic flow.

In this chapter, the distinction between regimes 1 and 2 in the headings for the different sections refers to the deformation behavior of quartz, not feldspar.

Experimentally deformed quartzo-feldspathic rocks

Further reading

Experimentally deformed quartzo-feldspathic rocks

starting & regime1 / regime 2 / annealing & melting

Dell'Angelo, L.N. and Tullis, J., 1996, Textural and mechanical evolution with progressive strain in experimentally deformed aplite. *Tectonophysics*, 256, 57-82.

Tullis, J., Dell'Angelo, L.N., and Yund, R.A., 1990, Ductile shear zones from brittle precursors in feldspathic rocks; the possible role of dynamic recrystallization: in *The Brittle-Ductile Transition: The Heard Volume*, A. Duba, W. Durham, J. Handin, and H. Wang, eds., Amer. Geophys. Union Monograph 56, 67-82.

Tullis, J. and Gleason, G., 1998, Effects of static annealing on experimentally deformed quartzite and aplite, in *Fault-Related Rocks: A Photographic Atlas*. A. Snoke, J. Tullis & V. Todd, eds., Princeton Univ. Press, 462-463.

Dell'Angelo, L.N. and Tullis, J., 1988, An experimental study of the effect of partial melt on granitic aggregates deformed at high pressures and temperatures: *Jour. Met. Geol.*, 6, 495-516.

Experimentally deformed quartzo-feldspathic rocks

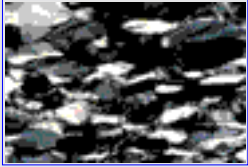
Regime 2

Experimentally
deformed
quartzo-feldspathic
rocks

starting material & regime1 / [regime 2](#) / annealing & melting

List of microstructures

57



[EA shortened 50% at 900°C, 10⁻⁶/sec, and 1200 MPa; quartz regime 2 dislocation creep and feldspars regime 1.](#)

58



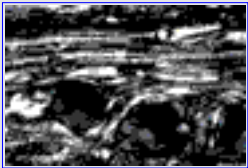
[EA shortened 60% at 900°C, 10⁻⁶/sec, and 1200 MPa; quartz becoming more interconnected, feldspars less so.](#)

59



[EA shortened 85% at 900°C, 10⁻⁶/sec, and 1200 MPa; recrystallized ribbons of quartz, feldspar augen with tails.](#)

61



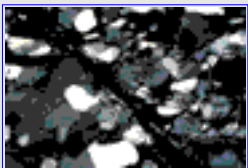
[EA shortened 40% and dextrally sheared \(\$\gamma = 2.4\$ \) at 900°C, 10⁻⁵/sec, and 1200 MPa; recrystallized ribbons of quartz, feldspar augen with tails.](#)

62



[EA shortened and dextrally sheared at 900°C, 10⁻⁶/sec, and 1200 MPa; recrystallized grain size of quartz is larger than feldspar.](#)

63



[EA pre-faulted at low P and T, then shortened 25% at 900°C, 10⁻⁶/sec, and 1200 MPa; high T deformation localized along former fault.](#)

Experimentally deformed quartzo-feldspathic rocks

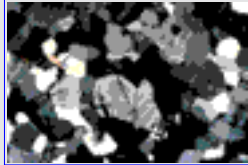
Starting material & regime 1

Experimentally
deformed
quartzo-feldspathic
rocks

[starting material & regime1](#) / [regime 2](#) / [annealing & melting](#)

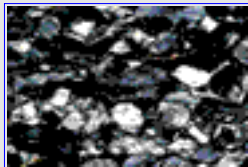
List of microstructures

55



[Enfield aplite \(EA\) starting material; ~30% quartz, ~35% microcline, ~35% oligoclase, and ~1% biotite.](#)

56



[EA shortened 35% at 725°C, 10-6/sec, and 1200 MPa; dispersed quartz \(regime 1\) was stronger than matrix feldspar \(cataclasis\).](#)

Experimentally deformed quartzo-feldspathic rocks

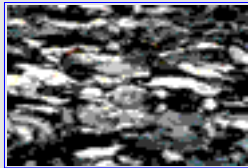
Annealing & melting

Experimentally deformed quartzo-feldspathic rocks

[starting material & regime 1](#) / [regime 2](#) / [annealing & melting](#)

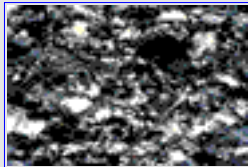
List of microstructures

64



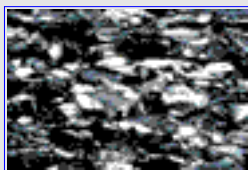
[EA shortened 60% at 800°C, 10⁻⁶/sec, and 1200 MPa; quartz regime 2 dislocation creep, feldspars semi-brittle flow \(compare with 65\).](#)

65



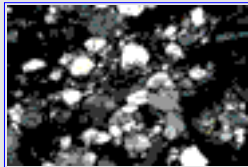
[EA shortened 60% at 800°C, 10⁻⁶/sec, and 1200 MPa \(same as 64\); then annealed at 900°C for 120 hrs.](#)

66



[EA shortened 67% at 900°C, 10⁻⁵/sec, and 1200 MPa with no melt; quartz regime 2 dislocation creep, feldspars semi-brittle \(compare with 67\).](#)

67



[EA shortened 67% at 900°C, 10⁻⁵/sec, and 1200 MPa; ~4% melt has resulted in cataclastic flow.](#)

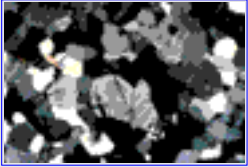
Experimentally deformed quartzo-feldspathic rocks

Figure caption

Experimentally
deformed
quartzo-
feldspathic rocks

[starting material & regime1](#) / [regime 2](#) / [annealing & melting](#)

55



Enfield aplite (EA) starting material; ~30% quartz, ~35% microcline, ~35% oligoclase, and ~1% biotite.

Enfield aplite (EA) starting material. This material comes from aplite dikes cutting the Black Mountain granite in Enfield, Vermont. The grain size is somewhat variable but averages ~200 μm . Quartz constitutes ~30%, microcline ~35% and oligoclase ~35%; there is about 1% biotite and magnetite. Because the two feldspars show very similar behavior in experimental deformation, this rock can be well approximated as a continuous stress-supporting matrix of feldspar with isolated, dispersed grains of quartz.

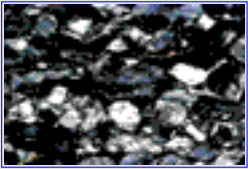
Experimentally deformed quartzo-feldspathic rocks

Figure caption

Experimentally
deformed
quartzo-
feldspathic rocks

starting material & regime1 / regime 2 / annealing & melting

56



EA shortened 35% at 725°C, 10⁻⁶/sec, and 1200 MPa; dispersed quartz (regime 1) was stronger than matrix feldspar (cataclasis).

EA shortened 35% at 725°C, 10⁻⁶/sec, 1200 MPa. At these conditions pure quartz aggregates deform by low temperature (regime 1) dislocation creep and are weaker than pure feldspar aggregates which deform by cataclastic flow. However, the texture in this aplite sample shows that the isolated quartz grains (mostly white grains) were stronger than the feldspar grains (mostly darker grey). The reason for this is that in regime 1 dislocation creep, the recovery process is bulging recrystallization, which can only occur if there are quartz-quartz grain boundaries - and these are rare in the aplite. (W352)

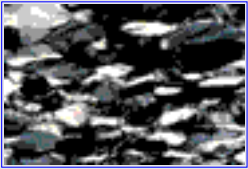
Experimentally deformed quartzo-feldspathic rocks

Figure caption

Experimentally deformed quartzo-feldspathic rocks

starting material & regime1 / regime 2 / annealing & melting

57



EA shortened 50% at 900°C, 10⁻⁶/sec, and 1200 MPa; quartz regime 2 dislocation creep and feldspars regime 1.

EA shortened 50% at 900°C, 10⁻⁶/sec, 1200 MPa. At these conditions the quartz deforms by intermediate temperature (regime 2) dislocation creep and the feldspars deform by low temperature (regime 1) dislocation creep. Because dislocation climb is easy in the quartz grains, they can undergo homogeneous grain flattening; some grains show sub-basal deformation lamellae, and recrystallized grains formed by progressive subgrain misorientation are observed especially along some grain boundaries. The feldspars are stronger and deform less homogeneously; they tend to undergo micro-boudinage, although that is not obvious in this photo. (W314)

Experimentally deformed quartzo-feldspathic rocks

Figure caption

Experimentally deformed quartzo-feldspathic rocks

[starting material & regime1](#) / [regime 2](#) / [annealing & melting](#)

58



EA shortened 60% at 900°C, 10⁻⁶/sec, and 1200 MPa; quartz becoming more interconnected, feldspars less so.

EA shortened 60% at 900°C, 10⁻⁶/sec, 1200 MPa. This photo shows a sample deformed at the same conditions as photo #57 but to higher strain. Here one can see better evidence for feldspar grains having been separated by boudinage into several smaller lozenge-shaped grains. Also, the continued homogeneous flattening of quartz grains has allowed them to become more interconnected (e.g. in SE quadrant of photo; also compare with the original grain size in photo 55). Thus with increasing strain at these conditions the feldspars tend to become less interconnected and the quartz tends to become more interconnected: the sample undergoes strain weakening as the bulk rock rheology switches from being more 'controlled' by the feldspars to being more 'controlled' by the quartz. (W304)

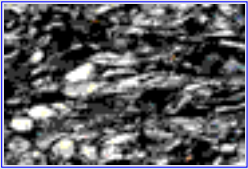
Experimentally deformed quartzo-feldspathic rocks

Figure caption

Experimentally
deformed
quartzo-
feldspathic rocks

starting material & regime1 / regime 2 / annealing & melting

59



EA shortened 85% at 900°C, 10⁻⁶/sec, and 1200 MPa; recrystallized ribbons of quartz, feldspar augen with tails.

EA shortened 85% at 900°C, 10⁻⁶/sec, 1200 MPa. This photo shows a sample deformed at the same conditions as photos #57 and 58 but to even higher strain. The remnants of feldspar grains (mostly darker grey) now appear as somewhat rounded augen with thin dark tails of very fine recrystallized grains formed by grain boundary bulging. The quartz grains (lighter grey and white) include flattened ribbons plus thin regions of coarser recrystallized grains formed by progressive subgrain rotation. (W323)

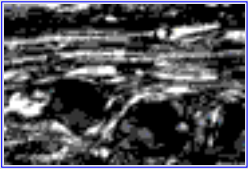
Experimentally deformed quartzo-feldspathic rocks

Figure caption

Experimentally
deformed
quartzo-
feldspathic rocks

starting material & regime1 / regime 2 / annealing & melting

61



EA shortened 40% and dextrally sheared ($\gamma = 2.4$) at 900°C, 10-5/sec, and 1200 MPa; recrystallized ribbons of quartz, feldspar augen with tails.

EA subjected to dextral shear ($\gamma = 2.4$, in a shear zone at 30 degrees to the external σ_1) plus compression (~40% shortening) at 900°C, 10-6/sec, 1200 MPa. The feldspar augen form sigma clasts, with asymmetric finely recrystallized tails. The quartz forms flattened ribbons. (W413)

Experimentally deformed quartzo-feldspathic rocks

Figure caption

Experimentally
deformed
quartzo-
feldspathic rocks

starting material & regime1 / regime 2 / annealing & melting

62



EA shortened and dextrally sheared at 900°C, 10⁻⁶/sec, and 1200 MPa; recrystallized grain size of quartz is larger than feldspar.

EA shortened 75% at 900°C, 10⁻⁶/sec, 1200 MPa. This view shows a region from near one corner of the sample where there has been dextral shearing around the piston. The feldspar augen form sigma clasts with recrystallized tails, and the quartz grains are flattened ribbons which are partially or completely recrystallized. In some places bands of more coarsely recrystallized quartz are separated by a thin dark seam of very finely recrystallized feldspar. In general, the recrystallized grains produced by grain boundary bulging (feldspar in this sample) are much smaller than those produced by progressive subgrain rotation (quartz in this sample). (W318)

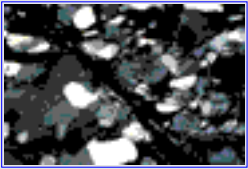
Experimentally deformed quartzo-feldspathic rocks

Figure caption

Experimentally deformed quartzo-feldspathic rocks

[starting material & regime1](#) / [regime 2](#) / [annealing & melting](#)

63



EA pre-faulted at low P and T, then shortened 25% at 900°C, 10⁻⁶/sec, and 1200 MPA; high T deformation localized along former fault.

EA pre-faulted at 300°C, 10⁻⁴/sec, 400 MPa and then taken to 900°C and 1200 MPA where it was shortened 25% at 10⁻⁶/sec. All of the high temperature deformation has been partitioned into the pre-existing fine-grained zone, due to the low temperature bulging recrystallization process in the feldspars. Recrystallization which occurs by subgrain misorientation does not produce strain weakening and thus does not result in preferential ductile shear in pre-existing fine-grained zones, as has been shown in experiments on pre-faulted quartzites. Note the coarser recrystallized grains of quartz adjacent to the shear zone in the bottom half of the photo. (W484)

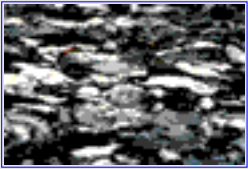
Experimentally deformed quartzo-feldspathic rocks

Figure caption

Experimentally
deformed
quartzo-
feldspathic rocks

[starting material & regime1](#) / [regime 2](#) / [annealing & melting](#)

64



EA shortened 60% at 800°C, 10⁻⁶/sec, and 1200 MPa; quartz regime 2 dislocation creep, feldspars semi-brittle flow (compare with 65).

EA shortened 60% at 800°C, 10⁻⁶/sec, 1200 MPa. At these conditions quartz deforms by regime 2 dislocation creep and the feldspar deformation is transitional from semi-brittle flow to regime 1 dislocation creep. Quartz grains (mostly white) are flattened, and the feldspar grains (darker) are less homogeneously deformed, with deformation bands and boudinage. Compare with annealed equivalent in photo 65. (W316)

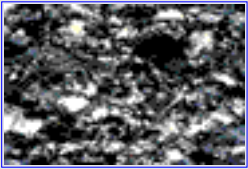
Experimentally deformed quartzo-feldspathic rocks

Figure caption

Experimentally
deformed
quartzo-
feldspathic rocks

[starting material & regime1](#) / [regime 2](#) / [annealing & melting](#)

65



EA shortened 60% at 800°C, 10⁻⁶/sec, and 1200 MPa (same as 64); then annealed at 900°C for 120 hrs.

EA deformed at exactly the same conditions as the sample shown in photo #64 and then hydrostatically annealed at 900°C for 120 hours. Many quartz grains show a necklace of coarse 'square' recrystallized grains. One feldspar grain shows evidence of multiple grain-scale faults. The recrystallized feldspar grains resulting from the anneal are much finer than the recrystallized quartz grains; some patches of recrystallized feldspar can be seen in the top right and left center of the photo. (AN5)

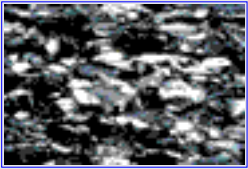
Experimentally deformed quartzo-feldspathic rocks

Figure caption

Experimentally
deformed
quartzo-
feldspathic rocks

starting material & regime 1 / regime 2 / annealing & melting

66



EA shortened 67% at 900°C, 10⁻⁵/sec, and 1200 MPa with no melt; quartz regime 2 dislocation creep, feldspars semi-brittle (compare with 67).

EA shortened 67% at 900°C, 10⁻⁵/sec, and 1200 MPa, with little or no melt present. Quartz deformed by regime 2 dislocation creep, feldspars deformed by semi-brittle flow (transitional between cataclastic flow and regime 1 dislocation creep). Compare with photo 67 to see the effect of melt. (PMA8)

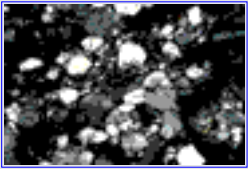
Experimentally deformed quartzo-feldspathic rocks

Figure caption

Experimentally
deformed
quartzo-
feldspathic rocks

starting material & regime1 / regime 2 / annealing & melting

67



EA shortened 67% at 900°C, 10⁻⁵/sec, and 1200 MPa; ~4% melt has resulted in cataclastic flow.

EA shortened 67% at 900°C, 10⁻⁵/sec, and 1200 MPa, with ~4% melt present (due to 1 wt % added water). The presence of the melt has changed the overall sample deformation to cataclastic flow. (PMA10)

6

Naturally deformed quartzo-feldspathic rocks

TOP

- | | |
|---|--|
| <u>1-</u> Experimentally deformed quartz aggregates | <u>2-</u> Naturally deformed quartz-rich rocks |
| <u>3-</u> Experimentally deformed feldspar aggregates | <u>4-</u> Naturally deformed feldspar rocks |
| <u>5-</u> Experimentally deformed quartzo-feldspathic rocks | <u>6-</u> Naturally deformed quartzo-feldspathic rocks |
| <u>7-</u> Experimentally deformed pyroxenite and diabase | <u>8-</u> Deformation and metamorphic reactions in polyphase rocks |

Naturally deformed quartzo-feldspathic rocks

weak deformation (Mulwarae) / strong deformation (Mulwarae) / mylonites (Redbank) / ultramylonites (Redbank)

Introduction

The samples illustrated in photos 68 to 76 were taken from a granodiorite cut by the Mulwarae fault zone, about 40 km east of Canberra, Australia. The samples represent stages of progressively higher shear strain found around less deformed boudins embedded in a more strongly deformed mylonitic matrix. Deformation occurred at mid-greenschist temperature conditions in the absence of significant amounts of aqueous fluids, because intermediate feldspars have remained chemically stable. Some alteration of feldspar to white mica is visible in these images but is due to later fracturing and fluid infiltration. Deformation has been accommodated by crystal plastic deformation in the quartz and biotite. Most of the feldspar in this rock is plagioclase, and plagioclase and K-feldspar are similar in their mechanical behavior; both deform only by fracturing at the relatively low temperatures of this deformation.

The samples illustrated in photos 77 to 87 were taken from the Redbank shear zone. The Redbank shear zone has a long history of activation through Proterozoic time, culminating with the development of mylonites during the late Paleozoic Alice Springs orogeny. This mylonite zone is several kilometers thick and is defined by a strong foliation and a prominent down-dip lineation. The Redbank shear zone contains the whole spectrum of mylonitic rocks, and pseudotachylite zones occur locally. Deformation at exposure level developed under greenschist-facies conditions.

Naturally deformed quartzo-feldspathic rocks

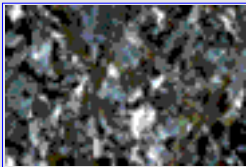
Weak deformation (Mulwaree fault zone, Australia)

Naturally
deformed
quartzo-feldspathic
rocks

weak deformation (Mulwaree) / strong deformation (Mulwaree) /
mylonites (Redbank) / ultramylonites (Redbank)

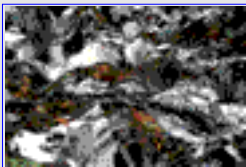
List of microstructures

68



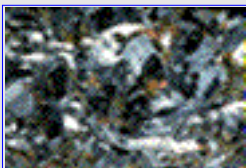
Granodiorite weakly deformed without reaction at mid greenschist conditions; feldspars fractured, quartz deformed by regime 2 dislocation creep.

69



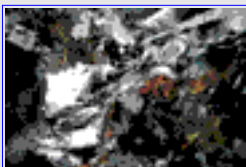
Detail of granodiorite weakly deformed at mid greenschist conditions.

70



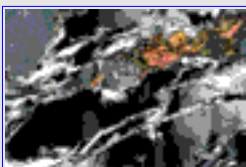
Granodiorite moderately deformed at mid greenschist conditions; feldspars fractured, quartz deformed by regime 2 dislocation creep.

71



Detail of granodiorite moderately deformed at mid greenschist conditions.

72



Detail of granodiorite moderately deformed at mid greenschist conditions.

Naturally deformed quartzo-feldspathic rocks

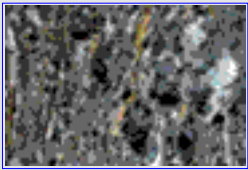
Strong deformation (Mulwaree fault zone, Australia)

Naturally
deformed
quartzo-feldspathic
rocks

weak deformation (Mulwaree) / strong deformation (Mulwaree) /
mylonites (Redbank) / ultramylonites (Redbank)

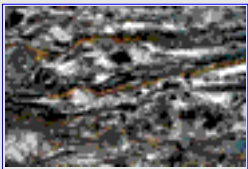
List of microstructures

73



Granodiorite highly deformed at mid greenschist conditions; fractured feldspars have separated, weaker quartz and biotite have coalesced.

74



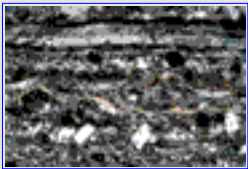
Detail of granodiorite highly deformed at mid greenschist conditions.

75



Granodiorite mylonite very highly deformed at mid greenschist conditions.

76



Detail of granodiorite mylonite deformed at mid greenschist conditions by fracturing of feldspars and coalescence of weaker quartz and biotite.

Naturally deformed quartzo-feldspathic rocks

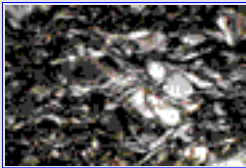
Mylonites (Redbank shear zone, Australia)

Naturally
deformed
quartzo-feldspathic
rocks

weak deformation (Mulwaree) / strong deformation (Mulwaree) /
mylonites (Redbank) / ultramylonites (Redbank)

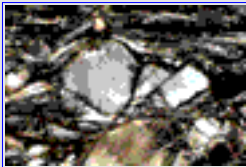
List of microstructures

77



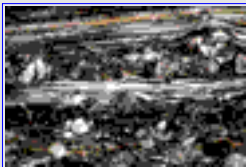
Quartzo-feldspathic mylonite developed at greenschist conditions; feldspars fractured, quartz deformed by regime 2 dislocation creep.

78



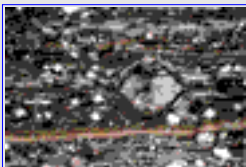
Detail of quartzofeldspathic mylonite, with fractured and rotated K feldspar.

79



Highly deformed quartzo-feldspathic mylonite; feldspars have fractured and separated, quartz has deformed by regime 2 dislocation creep.

80



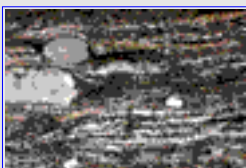
Detail of quartzofeldspathic mylonite, dextral shear.

81



Quartzo-feldspathic mylonite (same as 80); plane polarized light.

82



Quartzo-feldspathic mylonite developed at greenschist conditions; feldspar deformed by regime 1 dislocation creep, quartz by regime 2 dislocation creep.

Naturally deformed quartzo-feldspathic rocks

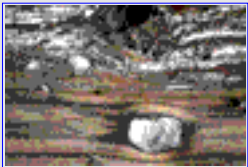
Ultramylonites (Redbank shear zone, Australia)

Naturally
deformed
quartzo-feldspathic
rocks

weak deformation (Mulwaree) / strong deformation (Mulwaree) /
mylonites (Redbank) / ultramylonites (Redbank)

List of microstructures

83



Gradation from mylonite to ultramylonite (UM) in aplite deformed at greenschist conditions; the UM matrix shows fine-scale phase mixing.

84



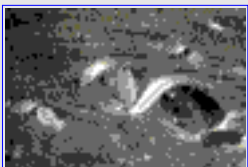
Quartzo-feldspathic ultramylonite; feldspar porphyroclast has asymmetrical tails of recrystallized or neo-mineralized grains.

85



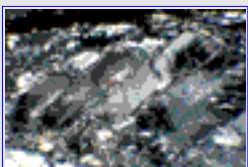
Quartzo-feldspathic ultramylonite (same as 84); rotated 45°.

86



Quartzo-feldspathic ultramylonite; feldspar porphyroclast has asymmetrical tails as well as white mica concentrations.

87



Quartzo-feldspathic ultramylonite; "bookshelf" feldspar has deformed by semi-brittle flow.

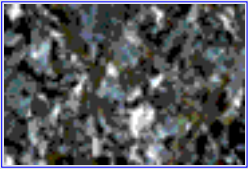
Naturally deformed quartzo-feldspathic rocks

Figure caption

Naturally
deformed
quartzo-feldspathic
rocks

weak deformation (Mulwaree) / high deformation (Mulwaree) /
mylonites (Redbank) / ultramylonites (Redbank)

68



Granodiorite weakly deformed without reaction at mid greenschist conditions; feldspars fractured, quartz deformed by regime 2 dislocation creep.

Overview of weakly deformed granodiorite. Quartz and biotite have deformed by intracrystalline plasticity processes, evident from the undulose extinction, subgrain formation, and dynamic recrystallization. Feldspars have deformed by fracturing.

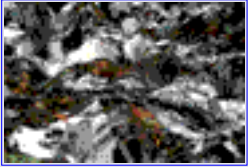
Naturally deformed quartzo-feldspathic rocks

Figure caption

Naturally
deformed
quartzo-feldspathic
rocks

weak deformation (Mulwaree) / high deformation (Mulwaree) / mylonites (Redbank) / ultramylonites (Redbank)

69



Detail of granodiorite weakly deformed at mid greenschist conditions.

Higher magnification view of the sample shown in photo #70, illustrating incipient recrystallization of quartz and biotite. Feldspar is undeformed at this low strain (the feldspar clast to the left of the image still shows igneous zoning). Quartz grains contain subgrains and some show core and mantle structures indicating the beginning of dynamic recrystallization by subgrain rotation (dislocation creep regime 2).

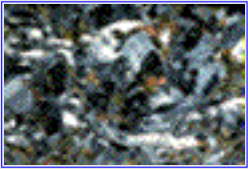
Naturally deformed quartzo-feldspathic rocks

Figure caption

Naturally deformed quartzo-feldspathic rocks

weak deformation (Mulwaree) / strong deformation (Mulwaree) / mylonites (Redbank) / ultramylonites (Redbank)

70



Granodiorite moderately deformed at mid greenschist conditions; feldspars fractured, quartz deformed by regime 2 dislocation creep.

Moderately deformed granodiorite; feldspars have fractured, quartz has deformed by regime 2 dislocation creep. There is a weak foliation defined by elongated and recrystallized aggregates of biotite and quartz.

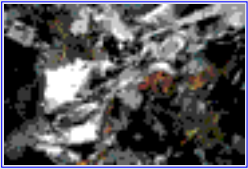
Naturally deformed quartzo-feldspathic rocks

Figure caption

Naturally
deformed
quartzo-feldspathic
rocks

weak deformation (Mulwaree) / strong deformation (Mulwaree) /
mylonites (Redbank) / ultramylonites (Redbank)

71



Detail of granodiorite moderately deformed at mid greenschist conditions.

Higher magnification view of moderately deformed granodiorite sample shown in photo #70. Near the center of the image, a rigid and relatively undeformed plagioclase porphyroclast has produced a stress concentration in the adjacent quartz grain, which is more strongly deformed (more prominent subgrain formation) near the plagioclase than further away from it.

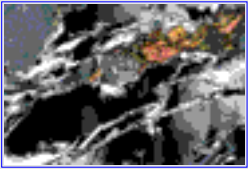
Naturally deformed quartzo-feldspathic rocks

Figure caption

Naturally
deformed
quartzo-feldspathic
rocks

weak deformation (Mulwaree) / strong deformation (Mulwaree) /
mylonites (Redbank) / ultramylonites (Redbank)

72



Detail of granodiorite moderately deformed at mid greenschist conditions.

Moderately deformed granodiorite. Elongated aggregates of recrystallized quartz and biotite have coalesced to form continuous layers. Feldspar porphyroclasts have deformed by brittle fracturing, without recrystallization or neomineralization; the new material that has formed between the feldspar fragments is quartz and biotite.

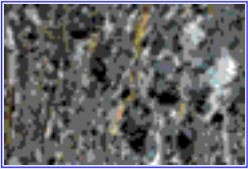
Naturally deformed quartzo-feldspathic rocks

Figure caption

Naturally deformed quartzo-feldspathic rocks

weak deformation (Mulwaree) / strong deformation (Mulwaree) / mylonites (Redbank) / ultramylonites (Redbank)

73



Granodiorite highly deformed at mid greenschist conditions; fractured feldspars have separated, weaker quartz and biotite have coalesced.

Strongly deformed granodiorite, illustrating foliation development. Dynamic recrystallization of quartz and biotite is concentrated near or between relatively rigid plagioclase porphyroclasts. Separation of feldspar fragments and coalescence of recrystallized quartz and biotite has begun to produce continuous layers of weak phases.

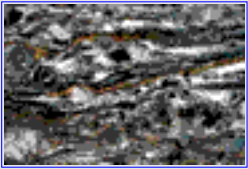
Naturally deformed quartzo-feldspathic rocks

Figure caption

Naturally
deformed
quartzo-feldspathic
rocks

weak deformation (Mulwaree) / strong deformation (Mulwaree) /
mylonites (Redbank) / ultramylonites (Redbank)

74



Detail of granodiorite highly deformed at mid greenschist conditions.

Higher magnification view of sample shown in photo #73. Protomylonitic granodiorite. Almost all the biotite has dynamically recrystallized and the quartz has been flattened into ribbon grains with substantial recrystallization by subgrain rotation (dislocation creep regime 2). Feldspar is present as clasts, fractured but not showing any traces of dynamic recrystallization or reaction. Coalescence of quartz and biotite has formed continuous weak layers.

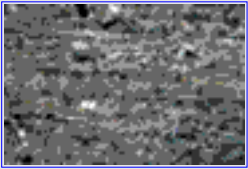
Naturally deformed quartzo-feldspathic rocks

Figure caption

Naturally
deformed
quartzo-feldspathic
rocks

weak deformation (Mulwaree) / strong deformation (Mulwaree) / mylonites (Redbank) / ultramylonites (Redbank)

75



Granodiorite mylonite very highly deformed at mid greenschist conditions.

Very high strain mylonite derived from granodiorite. The mylonite consists of continuous layers of dynamically recrystallized quartz and biotite, enveloping strings of feldspar porphyroclasts which have deformed by fracturing only.

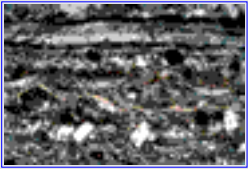
Naturally deformed quartzo-feldspathic rocks

Figure caption

Naturally deformed quartzo-feldspathic rocks

weak deformation (Mulwaree) / strong deformation (Mulwaree) / mylonites (Redbank) / ultramylonites (Redbank)

76



Detail of granodiorite mylonite deformed at mid greenschist conditions by fracturing of feldspars and coalescence of weaker quartz and biotite.

Higher magnification view of granodiorite mylonite shown in photo #75. Biotite is completely recrystallized and quartz is present as largely recrystallized ribbon grains; these two phases form continuous and almost planar layers over large distances. Most of the deformation is accommodated by these quartz and/or biotite layers. Fractured feldspar grains are concentrated in layers. The dominant deformation process in these granitoids is intracrystalline plasticity in weak monophase layers (quartz or biotite), which formed by gradual coalescence. Feldspar has not changed chemically and has not recrystallized, but deformed by fracturing.

Naturally deformed quartzo-feldspathic rocks

Figure caption

Naturally
deformed
quartzo-feldspathic
rocks

weak deformation (Mulwaree) / strong deformation (Mulwaree) /
mylonites (Redbank) / ultramylonites (Redbank)

77



Quartzo-feldspathic mylonite developed at greenschist conditions; feldpars fractured, quartz deformed by regime 2 dislocation creep.

Mylonite developed in quartzo-feldspathic aplite, deformed at greenschist grade in the Redbank shear zone. Quartz grains form thin ribbons wrapped around K-feldspar porphyroclasts. Some quartz ribbons may represent domains between kink bands rather than entire original grains. The ribbons contain well-developed subgrains and the recrystallized grains at their margins have approximately the same size, indicating deformation by dislocation creep regime 2. The feldspar porphyroclasts show some fracturing, the development of deformation-induced twin lamellae, and strong undulatory extinction. (499 A)

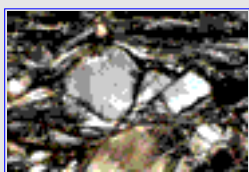
Naturally deformed quartzo-feldspathic rocks

Figure caption

Naturally
deformed
quartzo-feldspathic
rocks

weak deformation (Mulwaree) / strong deformation (Mulwaree) /
mylonites (Redbank) / ultramylonites (Redbank)

78



Detail of quartzite, with fractured and rotated K feldspar.

Higher magnification view of the sample shown in photo #77,
illustrating a fractured K-feldspar rotated in a 'bookshelf' manner
by dextral shear. (499A)

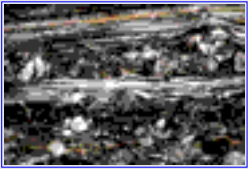
Naturally deformed quartzo-feldspathic rocks

Figure caption

Naturally
deformed
quartzo-feldspathic
rocks

weak deformation (Mulwaree) / strong deformation (Mulwaree) /
mylonites (Redbank) / ultramylonites (Redbank)

79



**Highly deformed quartzite-feldspathic
mylonite; feldspars have fractured and
separated, quartz has deformed by regime 2
dislocation creep.**

More highly deformed quartzite-feldspathic mylonite from the Redbank shear zone. Some layers are dominated by quartz ribbons and other layers contain fragments of broken feldspar surrounded by a fine-grained matrix of recrystallized quartz and cataclastic feldspar. (693 A)

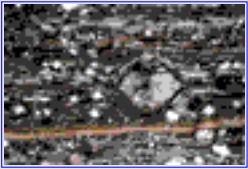
Naturally deformed quartzo-feldspathic rocks

Figure caption

Naturally
deformed
quartzo-feldspathic
rocks

weak deformation (Mulwaree) / strong deformation (Mulwaree) /
mylonites (Redbank) / ultramylonites (Redbank)

80



Detail of quartzo-feldspathic mylonite, dextral shear.

High magnification view of the quartzo-feldspathic mylonite shown in photo #79. Quartz forms partially recrystallized long ribbons and feldspar porphyroclasts show a range of sizes reflecting progressive grain-size reduction by fracturing. The imbricated nature of feldspar porphyroclasts is consistent with a dextral sense of shear. (495-4A)

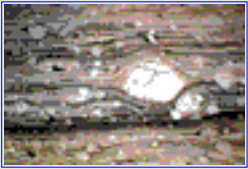
Naturally deformed quartzo-feldspathic rocks

Figure caption

Naturally
deformed
quartzo-feldspathic
rocks

weak deformation (Mulwaree) / strong deformation (Mulwaree) /
mylonites (Redbank) / ultramylonites (Redbank)

81



Quartzo-feldspathic mylonite (same as 80); plane polarized light.

Same view as photo #80, but in plane polarized light. Opaque minerals have been concentrated, by deformation and recrystallization, in the pressure shadows of some feldspar porphyroclasts and also along some foliae. (495-4A)

Naturally deformed quartzo-feldspathic rocks

Figure caption

Naturally
deformed
quartzo-feldspathic
rocks

weak deformation (Mulwaree) / strong deformation (Mulwaree) /
mylonites (Redbank) / ultramylonites (Redbank)

82



Quartzo-feldspathic mylonite developed at greenschist conditions; feldspar deformed by regime 1 dislocation creep, quartz by regime 2 dislocation creep.

Quartzo-feldspathic mylonite from the Redbank shear zone, showing the layering of quartz ribbons (regime 2 dislocation creep) and of small recrystallized or neo-mineralized feldspar grains. The new feldspar grains are concentrated in the pressure shadows of large porphyroclasts and strung out to form the mylonitic foliation. (495-10A)

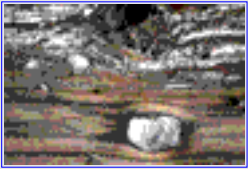
Naturally deformed quartzo-feldspathic rocks

Figure caption

Naturally deformed quartzo-feldspathic rocks

weak deformation (Mulwaree) / strong deformation (Mulwaree) / mylonites (Redbank) / ultramylonites (Redbank)

83



Gradation from mylonite to ultramylonite (UM) in aplite deformed at greenschist conditions; the UM matrix shows fine-scale phase mixing.

Contact between a mylonite and an ultramylonite in quartzo-feldspathic rock, from the Redbank shear zone. The ultramylonite matrix is very fine grained and composed of mixed quartz, mica, and K-feldspar with a large albite content. The relatively high mica content may be original but may also be due to the breakdown of K-feldspar. (599 A)

Naturally deformed quartzo-feldspathic rocks

Figure caption

Naturally
deformed
quartzo-feldspathic
rocks

weak deformation (Mulwaree) / strong deformation (Mulwaree) /
mylonites (Redbank) / ultramylonites (Redbank)

84



Quartzo-feldspathic ultramylonite; feldspar porphyroblast has asymmetrical tails of recrystallized or neo-mineralized grains.

Feldspar porphyroblast in ultramylonite from the same sample as shown in photo #83. The feldspar porphyroblast has asymmetric tails of recrystallized or neo-mineralized grains as well as an asymmetric concentration of white mica on the NW and SE sides (bright domains). This asymmetry indicate top-to-the-right sense of shear, consistent with other indicators in the rock. (599 A)

Naturally deformed quartzo-feldspathic rocks

Figure caption

Naturally
deformed
quartzo-feldspathic
rocks

weak deformation (Mulwaree) / strong deformation (Mulwaree) /
mylonites (Redbank) / ultramylonites (Redbank)

85



Quartzo-feldspathic ultramylonite (same as 84); rotated 45°.

Same area as photo #84, but rotated 45°. Now the white micas on the left and right sides of the porphyroclast are extinct, and thus difficult to distinguish from the feldspar tail, while the mica grains in the rest of the rock are bright. (599 A)

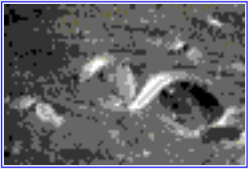
Naturally deformed quartzo-feldspathic rocks

Figure caption

Naturally
deformed
quartzo-feldspathic
rocks

weak deformation (Mulwaree) / strong deformation (Mulwaree) /
mylonites (Redbank) / ultramylonites (Redbank)

86



Quartzo-feldspathic ultramylonite; feldspar porphyroclast has asymmetrical tails as well as white mica concentrations.

Ultramylonite from the same rock illustrated in photo #83. Several K-feldspar porphyroclasts in a fine-grained matrix of quartz-mica-feldspar. Asymmetric tails of recrystallized or neo-mineralized feldspar as well as asymmetric concentrations of white mica on the NW and SE sides of the grains indicate top-to-the-right shear. (599 A)

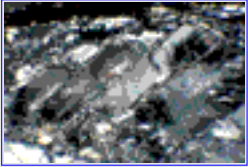
Naturally deformed quartzo-feldspathic rocks

Figure caption

Naturally
deformed
quartzo-feldspathic
rocks

weak deformation (Mulwaree) / strong deformation (Mulwaree) /
mylonites (Redbank) / ultramylonites (Redbank)

87



Quartzo-feldspathic ultramylonite; "bookshelf" feldspar has deformed by semi-brittle flow.

"Bookshelf" feldspar in quartzite-feldspathic mylonite from the Redbank shear zone. The shear zones between the "books" contain recrystallized or neo-mineralized feldspar grains 15 μm in diameter (435 A)

7

Experimentally deformed pyroxenite and diabase

TOP

- | | |
|---|--|
| <u>1-</u> Experimentally deformed quartz aggregates | <u>2-</u> Naturally deformed quartz-rich rocks |
| <u>3-</u> Experimentally deformed feldspar aggregates | <u>4-</u> Naturally deformed feldspar rocks |
| <u>5-</u> Experimentally deformed quartzo-feldspathic rocks | <u>6-</u> Naturally deformed quartzo-feldspathic rocks |
| <u>7-</u> Experimentally deformed pyroxenite and diabase | <u>8-</u> Deformation and metamorphic reactions in polyphase rocks |

Experimentally deformed pyroxenite and diabase

examples

Introduction

In rocks of the granitic continental crust, mica and quartz are the weaker phases and feldspars are the stronger phase, but in rocks of the gabbroic oceanic crust, the feldspars are generally the weaker phase and pyroxenes are the stronger phase. The deformation microstructures developed in deformed pyroxenites have not been as thoroughly studied experimentally as those in quartz and feldspar (and olivine), but this mineral appears to undergo a similar sequence of dislocation creep regimes. In this chapter we include images of two different experimentally deformed samples, which seem to show microstructures characteristic of regime 1 and regime 2 dislocation creep. In addition, we include an image of a fine-grained gabbro (diabase) experimentally deformed to high strain, which shows pyroxene 'augen' and highly flattened plagioclase feldspar grains, similar to microstructures observed in some natural mylonites.

[further reading](#)

Experimentally deformed pyroxenite and diabase

Further reading

Experimentally
deformed
pyroxenite and
diabase

examples

Tullis, T.E., Horowitz, F.E. and Tullis, J., 1991, Flow laws of polyphase aggregates from end member flow laws. Jour. Geophys. Res., 96, 8081-8096.

Kronenberg, A.K. and Shelton, G.S., 1980, Deformation microstructures in experimentally deformed Maryland diabase. Jour. Struct. Geol., 2, 341-353.

Experimentally deformed pyroxenite and diabase

Experimentally deformed pyroxenite and diabase

[examples](#)

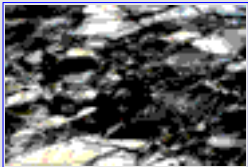
List of microstructures

88



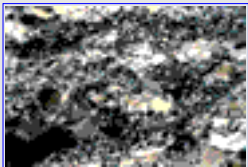
[Sleaford Bay diopside \(SBD\) starting material.](#)

89



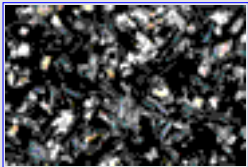
[SBD shortened 52% at 1100°C, 10⁻⁵/sec and 1200 MPa; regime 2 dislocation creep.](#)

90



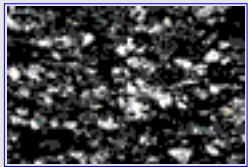
[SBD shortened 32% at 1200°C, 10⁻⁶/sec and 1200 MPa; regime 3 dislocation creep.](#)

91



[Maryland diabase \(MD\) starting material; ~35% plagioclase, ~60% clinopyroxene, ~5% opaques and chlorite.](#)

92



[MD shortened 50% at 1000°C, 10⁻⁴/sec and 1200 MPa; pyroxene is stronger and forms augen.](#)

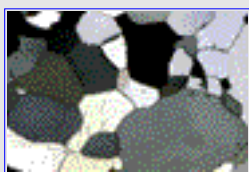
Experimentally deformed pyroxenite and diabase

Figure caption

Experimentally
deformed
pyroxenite and
diabase

examples

88



Sleaford Bay diopside (SBD) starting material.

Sleaford Bay diopside (SBD) starting material from Australia. Mg:Ca:Fe is 40:50:10. Average grain size is ~300 μm ; some grains contain twins on (100) and (001). Section is extra thin.

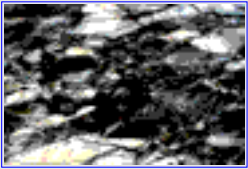
Experimentally deformed pyroxenite and diabase

Figure caption

Experimentally deformed pyroxenite and diabase

examples

89



SBD shortened 52% at 1100°C, 10⁻⁵/sec and 1200 MPa; regime 2 dislocation creep.

SBD shortened 52% at 1100°C, 10⁻⁵/sec, and 1200 MPa. Deformation has involved some flattening of original grains, with fine recrystallized grains developed along grain boundaries and along internal twin boundaries. (W590)

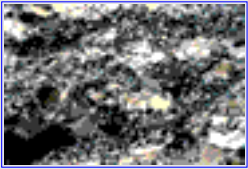
Experimentally deformed pyroxenite and diabase

Figure caption

Experimentally deformed pyroxenite and diabase

examples

90



SBD shortened 32% at 1200°C, 10⁻⁶/sec and 1200 MPa; regime 3 dislocation creep.

SBD shortened 32% at 1200°C, 10⁻⁶/sec, and 1200 MPa. At this higher temperature the recrystallized grains are larger and more numerous for a given strain, and original grains are less obviously flattened. Subgrains are visible within original grains. (W589)

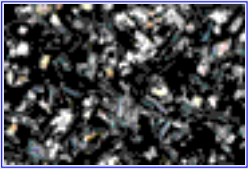
Experimentally deformed pyroxenite and diabase

Figure caption

Experimentally
deformed
pyroxenite and
diabase

examples

91



**Maryland diabase (MD) starting material;
~35% plagioclase, ~60% clinopyroxene, ~5%
opaques and chlorite.**

Maryland diabase (MD) starting material. This material is composed of ~35% plagioclase (An₇₁) and ~60% clinopyroxene (En₄₆Wo₃₈Fs₁₆), with ~5% opaques and chlorite. The plagioclase and the clinopyroxene are about equally interconnected. The average grain size is ~100 μm .

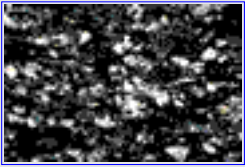
Experimentally deformed pyroxenite and diabase

Figure caption

Experimentally deformed pyroxenite and diabase

examples

92



MD shortened 50% at 1000°C, 10⁻⁴/sec and 1200 MPa; pyroxene is stronger and forms augen.

MD shortened 50% at 1000°C, 10⁻⁴/sec, and 1200 MPa (roughly equivalent to 800°C and 10⁻⁶/sec, for comparison to experimentally deformed samples of pure feldspar aggregates and quartzo-feldspathic rocks). At these conditions the pyroxene is the stronger phase and remains as relatively undeformed augen, and the plagioclase has undergone semi-brittle flow, including grain-scale faulting, which has allowed the laths to become strongly aligned. Thus at the same experimental deformation conditions, feldspar is the stronger phase in granite but the weaker phase in diabase. (W269)

8

Deformation and metamorphic reactions in polyphase rocks

TOP

- | | |
|---|--|
| <u>1-</u> Experimentally deformed quartz aggregates | <u>2-</u> Naturally deformed quartz-rich rocks |
| <u>3-</u> Experimentally deformed feldspar aggregates | <u>4-</u> Naturally deformed feldspar rocks |
| <u>5-</u> Experimentally deformed quartzo-feldspathic rocks | <u>6-</u> Naturally deformed quartzo-feldspathic rocks |
| <u>7-</u> Experimentally deformed pyroxenite and diabase | <u>8-</u> Deformation and metamorphic reactions in polyphase rocks |

Deformation and metamorphic reactions

granodiorites / anorthosites

Introduction

The samples illustrated in photos 93 to 98 represent progressively deformed granodiorite from the Corvatsch shear zone at Corvatsch in the Engadine, Swiss Alps. Deformation occurred at 250 to 400°C (lower to mid greenschist facies conditions). Deformation in these rocks involved grain boundary sliding and/or diffusion creep, facilitated by the breakdown of plagioclase to a fine grained aggregate of albite + epidote +/- white mica +/- quartz. The grain size within this mixed-phase assemblage is 2 to 20 µm.

The anorthosite samples come from the same shear zone as the samples of naturally deformed feldspar rocks shown in chapter 4 (Jotun nappe, Norway).

[further reading](#)

Deformation and metamorphic reactions in polyphase rocks

Further reading

Deformation and metamorphic reactions / granodiorites / anorthosites

Fitz Gerald, J.D. and Stunitz, H., 1993, Deformation of granitoids at low metamorphic grade. I. Reactions and grain size reduction. *Tectonophys.*, 221, 269-297.

Kruse, R., and Stunitz, H., 1999, Deformation mechanisms and phase distribution in mafic high-temperature mylonites from the Jotun Nappe, southern Norway. *Tectonophys.*, 303, 223-249.

Stunitz, H. and Tullis, J., Weakening and strain localization produced by syndeformational reaction of plagioclase. In press, *Geol. Rundsch.*

Stunitz, H., 1993, Transition from fracturing to viscous flow in a naturally deformed metagabbro. in *Defects and Processes in the Solid State: Geoscience Applications*, J.N. Boland and J.D. Fitz Gerald, eds., Elsevier, Amsterdam, 121-150.

Stunitz, H. and Fitz Gerald, J.D., 1993, Deformation of granitoids at low metamorphic grades. II. Granular flow in albite-rich mylonites. *Tectonophys.*, 221, 299-324.

Stunitz, H., 1998, Syn-deformational recrystallization - dynamic or compositionally induced? *Contrib. Mineral. Petrol.*, 131, 219-236.

Deformation and metamorphic reactions in polyphase rocks

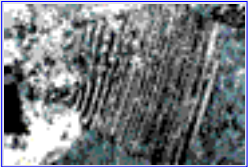
Granodiorites

Deformation and metamorphic reactions

granodiorites / anorthosites

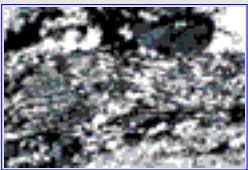
List of microstructures

93



Plagioclase grain from granodiorite weakly deformed at low to mid greenschist conditions; recrystallization involved change of composition.

94



Plagioclase grain from granodiorite moderately deformed at low to mid greenschist conditions, and mostly reacted to a mixture of albite and clinozoisite.

95



Mylonite derived from granodiorite at low to mid greenschist conditions; reaction plus deformation produced a weak fine grained mixed phase matrix.

96



Granodiorite mylonite deformed at low to mid greenschist conditions; pure quartz layers are stronger than mixed phase matrix.

97



Granodiorite mylonite (same as 96), plane polarized light.

98



Detail of granodiorite mylonite; pure quartz regions deformed by regime 3 dislocation creep; fine grained mixed phase matrix deformed by grain boundary sliding - diffusion creep.

Deformation and metamorphic reactions in polyphase rocks

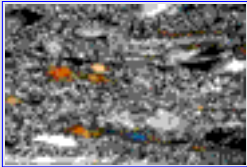
Anorthosites

Deformation and metamorphic reactions

granodiorites / anorthosites

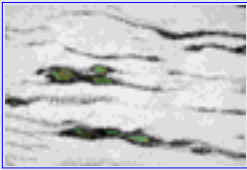
List of microstructures

99



Anorthosite deformed at granulite grade; plagioclase deformed by regime 2 dislocation creep, and recrystallized grains have same composition as host.

100



Anorthosite deformed at granulite grade (same as 99), plane polarized light; heterogeneous nucleation of hornblende between plagioclase grains.

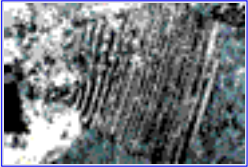
Deformation and metamorphic reactions in polyphase rocks

Figure caption

Deformation and metamorphic reactions

granodiorites / anorthosites

93



Plagioclase grain from granodiorite weakly deformed at low to mid greenschist conditions; recrystallization involved change of composition.

Weakly deformed granodiorite. Recrystallization of plagioclase has occurred along fractures which do not show major displacement. The left part of the porphyroclast is substantially recrystallized; the composition of the new grains is albite, whereas the host grain is an intermediate plagioclase. The recrystallization occurs through nucleation of new grains with a different chemical composition from that of the host grain; thus, it is better termed neo-mineralization. Small light specks are white mica, and the high-relief mineral is clinozoisite.

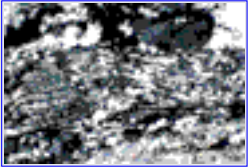
Deformation and metamorphic reactions in polyphase rocks

Figure caption

Deformation and metamorphic reactions

granodiorites / anorthosites

94



Plagioclase grain from granodiorite moderately deformed at low to mid greenschist conditions, and mostly reacted to a mixture of albite and clinozoisite.

More strongly deformed granodiorite, showing a plagioclase grain which has been largely decomposed by neo-mineralization. Mixtures of very fine-grained high-relief clinozoisite and albite are beginning to form interconnected layers, leading to a foliation in the rock. In the upper part of the image, quartz is dynamically recrystallized with a grain size larger than that in the phase mixture.

Deformation and metamorphic reactions in polyphase rocks

Figure caption

Deformation and metamorphic reactions

granodiorites / anorthosites

95



Mylonite derived from granodiorite at low to mid greenschist conditions; reaction plus deformation produced a weak fine-grained mixed phase matrix.

Mylonite derived from granodiorite. The matrix consists of fine-grained albite + epidote + quartz. Most of the deformation has been accommodated by this phase mixture. Quartz porphyroclasts embedded in this matrix show incipient dynamic recrystallization, with a grain size larger than the grain size of the phase mixture. TEM shows no dislocations in the highly strained fine grained phase mixture; thus the dominant deformation mechanism is inferred to be grain boundary sliding and diffusion creep.

Deformation and metamorphic reactions in polyphase rocks

Figure caption

Deformation and metamorphic reactions

granodiorites / anorthosites

96



Granodiorite mylonite deformed at low to mid greenschist conditions; pure quartz layers are stronger than mixed phase matrix.

Overview of a granodiorite mylonite. The monophase layers of quartz are more competent (pinch and swell structures, boudinage) than the fine-grained mixture of albite + epidote + quartz + white mica matrix. Photo 97 (plane polarized light) shows that quartz forms more or less pure, monophase layers. This competence reversal between quartz and feldspar-dominated layers indicates that the matrix has not deformed by intracrystalline plasticity, because quartz (which is dynamically recrystallized, and thus deformed by crystal plastic mechanisms) forms the mechanically stronger aggregates, and pure albite at these temperatures deforms by brittle fracturing.

Deformation and metamorphic reactions in polyphase rocks

Figure caption

Deformation and metamorphic reactions

granodiorites / anorthosites

97



Granodiorite mylonite (same as 96), plane polarized light.

Plane polarized light view of a granodiorite mylonite showing that monophase layers of quartz are more competent than the fine-grained matrix, as evidenced by their pinch and swell boudinage.

Deformation and metamorphic reactions in polyphase rocks

Figure caption

Deformation and metamorphic reactions

granodiorites / anorthosites

98



Detail of granodiorite mylonite; pure quartz regions deformed by regime 3 dislocation creep while fine-grained mixed phase matrix deformed by grain boundary sliding - diffusion creep.

Detail of granodiorite mylonite. The fine-grained portions consist of a mixture of albite + epidote/clinozoisite + quartz + white mica. The coarse-grained portion consists of pure quartz, which is dynamically recrystallized by regime 3 dislocation creep. The phase mixture has a finer grain size due to rapid nucleation of new phases and grain boundary pinning, and this finer grain size allowed a switch to grain boundary sliding and diffusion creep.

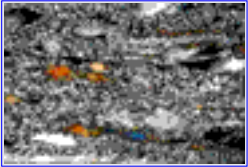
Deformation and metamorphic reactions in polyphase rocks

Figure caption

Deformation and metamorphic reactions

granodiorites / anorthosites

99



Anorthosite deformed at granulite grade; plagioclase deformed by regime 2 dislocation creep, and recrystallized grains have same composition as host.

This image and image #100 illustrate a similar mechanism for the formation of mixed phase aggregates as shown above in a granitoid (images 93-98) but at higher temperatures in an anorthosite (700°C, same rock as images 49-54). These images of largely recrystallized anorthosite from Norway illustrate a difference in the recrystallization process for plagioclase and hornblende.

Plagioclase porphyroclasts have tails consisting of monophase plagioclase domains. The new grains in the tails have the same composition as the porphyroclasts, indicating that they formed by dynamic recrystallization. Conversely, the tails extending from hornblende porphyroclasts are mixed phase aggregates of hornblende and plagioclase. The phase mixture may be due to heterogeneous nucleation of hornblende between plagioclase grains. This mechanism is consistent with the observed small change in composition between old and new hornblende grains.

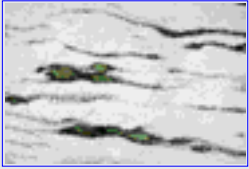
Deformation and metamorphic reactions in polyphase rocks

Figure caption

Deformation and metamorphic reactions

granodiorites / anorthosites

100



Anorthosite deformed at granulite grade (same as 99), plane polarized light; heterogeneous nucleation of hornblende between plagioclase grains.

Plane polarized light view of image #99. Note the small hornblende grains which appear to have nucleated heterogeneously between plagioclase grains. These new hornblende grains have a composition slightly different from that of the hornblende porphyroclasts.